The Thesis Committee for Bong Wan Jun
Certifies that this is the approved version of the following thesis:

An Investigation on Transmitter and Receiver Diversity for Wireless Power Transfer

APPROVED BY
SUPERVISING COMMITTEE:

Supervisor:

____
Hao Ling

____
Andrea Alù

An Investigation on Transmitter and Receiver Diversity for Wireless Power Transfer

by

Bong Wan Jun, B. S.

Thesis

Presented to the Faculty of the Graduate School of

The University of Texas at Austin

in Partial Fulfillment

of the Requirements

for the Degree of

Master of Science in Engineering

The University of Texas at Austin

May 2011

Acknowledgements

First of all, I would like to express my deepest appreciation to my advisor, Professor Hao Ling, for his distinguished advice, support, and trust directed towards me. This thesis would not have been possible without him. I am also grateful to Professor Andrea Alù for being the reader of my thesis. His lectures were important sources to understand the background theory for this thesis. I would like to extend my gratitude to my lab colleagues for their support and advice, especially to Ick-Jae Yoon and Shang-Te Yang. I also thank Nicholas Whitelonis, Aale Naqvi, and Blake Levy for helping the grammar in this thesis. Finally, I would like thank my family and my wife, Yoonjung, for their support.

May 2011

Abstract

An Investigation on Transmitter and Receiver Diversity for Wireless Power Transfer

Bong Wan Jun, M.S.E.

The University of Texas at Austin, 2011

Supervisor: Hao Ling

This thesis investigates near-field wireless power transfer using multiple transmitters or multiple receivers. First, transmitter diversity is investigated in terms of the power transfer efficiency (PTE). It is found that an improvement in the PTE can be achieved by increasing the number of transmitters. Furthermore, a region of constant PTE can be created with the proper arrangement of transmitters.

Next, receiver diversity is investigated in detail. An improvement in the PTE can be also achieved by increasing the number of receivers. However, it is shown that when two or more receivers are closely located, the PTE is reduced due to mutual coupling between receivers. This is termed a 'sink' phenomenon, and it is investigated through measurement and simulation.

Finally, to account for more general situations of multiple transmitters and multiple receivers, Monte-Carlo simulation is applied. The cumulative distribution function (CDF) is used to interpret the results of the Monte-Carlo simulation. The transmitter and receiver diversity gain can be found based on the CDF. Moreover, the sink phenomenon can be observed by analyzing the CDF curve. Several strategies for positioning receivers are introduced to reduce the sink phenomenon. The results of the Monte-Carlo simulation also show that a saturation in the transmitter or receiver gain is reached when the number of transmitters or receivers is increased. Therefore, increasing the number of transmitters or receivers beyond a certain number does not help increase the PTE.

Table of Contents

List of Tables

List of Figures

Chapter 1 : Introduction

The concept of wireless power transfer has been applied to numerous applications. For example, power transferring surfaces have been implemented upon which small robots can move without batteries [1]-[3]. A planar surface has also been used as a contactless battery charging platform [4], [5]. Moreover, in terms of the size of power transferring devices, there have been a number of works which showed potential for wirelessly powering small implantable biomedical devices [6]-[8] as well as bigger objects such as vehicles [9], [10].

Wireless power transfer can be categorized based upon the region it is effective measured in terms of wavelength. Depending on the distance, the regions can be approximately divided into an inductive coupling region, a resonance coupling region, a near-field region, and a far-field region. Many earlier works used the inductive coupling approach. However, this requires transmitters and receivers to be in close proximity of each other. There have been various efforts to transfer power to the far-field region using a narrow antenna beam as early as the 1960s [11]-[13]. For example, a wirelessly powered helicopter was demonstrated for 10 hours [14]. The concept of solar power satellite (SPS) was also explored [15]. To reach far distance with good efficiency, narrow beams or highly directive antennas are needed. This means that the antennas must be electrically large. Without a narrow beam, the received power through the far-field region is low [16].

The magnetic resonance coupling has drawn attention of researchers since it showed the capability of wireless power transfer over longer range than the inductive coupling [17], [18]. The coupled mode region of electrically small antennas has been investigated using a meander antenna [19]. It was shown that high power transfer efficiency (PTE) can be achieved in this coupled mode region. However, it is not easy to design an antenna with an extended coupled mode region to reach longer distance in terms of wavelength [20].

Beyond the coupled mode region, a radiative near-field region has been also investigated [21], [22]. The PTE in the near-field region has a rapid decay rate as a function of distance. However, a sufficiently high PTE can still be achieved in this region for it to be of interest. A theoretical upper bound in PTE was derived for electrically small antennas with high radiation efficiency in [21]. Subsequently, folded cylindrical helix (FCH) antennas were designed and measured to show that the theoretical bound can be approached in practice [22]-[24].

The interests for wireless power transfer have also been extended to the case of multiple transmitters or multiple receivers. There have been a number of works concerning multiple elements in wireless power transfer. As an extension of [17], a wireless power transfer to multiple receivers has been investigated using magnetic resonance coupling [26]. It was shown that the overall PTE increases due to the additional receiver. As an extension of [22], the PTE of multiple transmitters and a single receiver has also been investigated in the near-field region using FCH dipoles [27]. It was shown through simulation and measurement that the overall PTE also increased due to an additional transmitter.

However, most previous works have paid attention to limited configurations regarding multiple transmitters and multiple receivers. First, the location of multiple elements has been constrained. Only one-dimensional variation for transmitters or receivers has been applied in [26] and [27]. In this way, the results can be shown as a simple PTE versus distance plot, but it cannot account for more general situations of locating multiple elements. Moreover, there has been no detailed consideration for mutual coupling between multiple elements, which may cause degradation in the PTE instead of an improvement by adding more transmitters or receivers. Finally, more investigation on the PTE gain is required. For example, while the PTE can be increased with additional transmitters or receivers, it is not known whether the PTE will saturate beyond a certain number of elements.

The main objective of this thesis is to investigate wireless power transfer using multiple transmitters and multiple receivers in the near-field region. The thesis is organized as follows. In Chapter 2, the case of multiple transmitters and a single receiver is analyzed. Two kinds of configurations for multiple transmitters are used, followed by a discussion of the transmitter gain. In Chapter 3, the case of a single transmitter and multiple receivers is investigated in detail. Two different configurations for locating receivers are applied. It is found that degradation of PTE exists as well as a receiver gain when two or more receivers are closely located. This phenomenon is termed as a 'sink' phenomenon. One-dimensional simulation is designed to investigate the sink phenomenon in more detail. The result is supported by measurements. Furthermore, to find what causes the sink phenomenon, a local search on the load impedance of a receiver is performed. In Chapter 4, Monte-Carlo simulation is applied to account for more general situations under unconstrained receiver locations. The simulation setup is introduced with an example to interpret the simulation results with cumulative distribution function (CDF) curves. As a way to reduce the sink phenomenon, a number of constraints on positioning receivers are applied. With resulting data from the Monte-Carlo simulation, the transmitter and receiver gains by using multiple transmitters and receivers are discussed. It is followed by a discussion of the saturation in the transmitter and receiver diversity gain.

Chapter 2: Transmitter Diversity with a Single Receiver

In this chapter, we study wireless power transfer in the case of multiple transmitter with a single receiver. Comparing to the case of a single transmitter and a single receiver, it is shown that there is an improvement in the PTE, termed a transmitter gain, due to added transmitters. This chapter begins with the methodology behind simulations using the Numerical Electromagnetics Code (NEC). First, wireless power transfer of the case of a single transmitter and a single receiver is investigated. Next, the case of multiple transmitters and a single receiver is investigated to find the transmitter gain. Two configurations for locating multiple transmitters are presented to investigate the transmitter gain. In the first configuration, two transmitters are fixed at both sides of a single receiver, and the receiver varies its positions between them. In the second configuration, a single receiver is fixed at the center around which multiple transmitters are located, increasing their distances.

2. 1. NEC SETUP

The power transfer efficiency (PTE) is defined as the ratio of the dissipated power at the load of the receiving antennas (Rx) to the accepted power at the transmitting antennas (Tx), described in Eq (1). For all simulations and measurements, transmitters and receivers correspond to input ports and output ports in an N-port network respective-

$$PTE = \frac{\sum_{i}^{\#\text{ of Rx}} P_{\text{Dissipated at Rx }(i)}}{\sum_{j}^{\#\text{ of Tx}} P_{\text{Accepted at Tx }(j)}} \tag{1}$$

ly, illustrated in Figure 1. In NEC, a short dipole antenna with a length of λ/50 and a small radius (0.01mm) is used. An electrically small, short dipole antenna is considered for an appropriate comparison to theory [21]. This also increases simulation speed in NEC. Each transmitter is excited with 1[V] in-phase and each receiver is loaded with a complex load impedance Z_L[Ω]. Therefore, the accepted power at the transmitter and the dissipated power at the receiver can be calculated as shown in Eq. (2), where I_{ZL} is the terminal current at the load and I_{in} is the current at the input port which are obtained using NEC simulation.

$$P = \frac{1}{2}\mathrm{Re}[VI^*] = \begin{cases} \frac{1}{2}\left|I_{Z_L}\right|^2 \mathrm{Re}[Z_L] & \text{for Rx} \\ \frac{1}{2}\mathrm{Re}[I_{in}{}^*] & \text{for Tx } (\because V = 1 + j0 \text{ in NEC}) \end{cases} \tag{2}$$

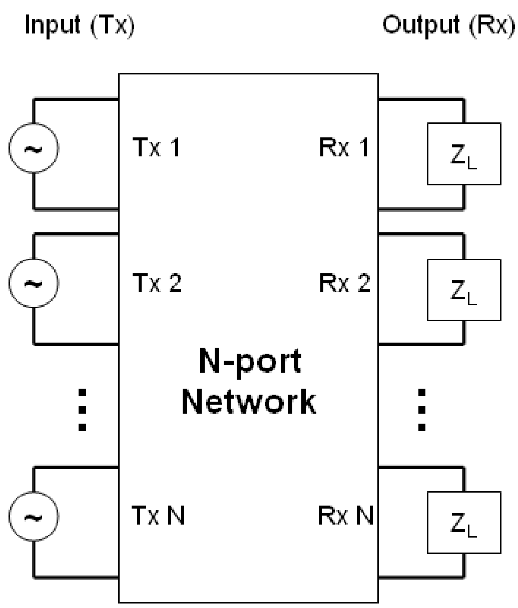

Figure 1. N-port network description of multiple Tx and multiple Rx antennas

Figure 2. Antenna alignment. (a) Parallel configuration, (b) Co-linear configuration

Since dipole antennas are not isotropic, an antenna alignment should be considered and have consistency throughout simulation and measurement. The possible two considerations are parallel and co-linear configurations as shown Figure 2. In this thesis, only the parallel configuration is considered.

2. 2. SINGLE TX SINGLE RX

To investigate the case of multiple transmitters and multiple receivers, the case of a single transmitter and a single receiver is investigated first. The resulting PTEs are depicted in Figure 3. For the blue curve, in order to find an appropriate value of the load impedance of the receiver to reach the maximum PTE, a local search was performed at every point. The fixed load impedance was used for the red curve. The value of the fixed complex load impedance is 0.109992 + j0.149322E+05, which was determined by a conjugate of the antenna input impedance. This is the optimum value of the load impedance when two antennas are very far apart [29]. The operating frequency was set to 200 MHz for the consistency with FCH dipoles [22]. FCH dipoles are more implementable in practice compared to short dipoles since the input impedance is close to 50 Ω.

In Figure 3, the two lines show good agreement with Friis transmission equation [30]. In Eq. (3), the polarization effect has been ignored and efficiencies for a transmitter and a receiver are all assumed to be 100% because perfect electric conductor (PEC) is used in the NEC simulation. The transmitter mismatch loss($1 - |\Gamma_t|^2$) does not need to be considered since PTE deals with an accepted power which is described by (Available power at Tx) x (Tx mismatch loss) according to the definition of PTE. The receiver mismatch loss is zero because $Z_A = Z_L^*$ in Eq. (4). When the load impedance is complex, Eq. (4) should be used and it is clear that when the receiver is matched to complex conjugate of its input impedance, Eq. (4) becomes unity, which means zero mismatch loss [31].

$$P_r = \left(1 - |\Gamma_t|^2\right)\left(1 - |\Gamma_r|^2\right)\left(\frac{\lambda}{4\pi R}\right)^2 \mathrm{D_t D_r} \tag{3}$$

Γ_t : Reflection coefficient of Tx

Γ_r : Reflection coefficient of Rx

P_t, P_r : Transmitted, received power

D_t, D_r : Directivity of Tx and Rx

R : Distance between Tx and Rx

$$1 - |\Gamma_r|^2 = \frac{4\,\mathrm{Re}[Z_A]\,\mathrm{Re}[Z_L]}{|Z_A + Z_L|^2} \tag{4}$$

Z_A : Antenna input impedance, Z_L : Load impedance

Before we proceed to the case of multiple transmitters and multiple receivers, it is important to consider that adding more transmitter or receiver gives rise to additional degrees of freedom. In Figure 4. (a), we need only to consider the distance between a single transmitter and a single receiver for the 1Tx 1Rx case. However, adding one more

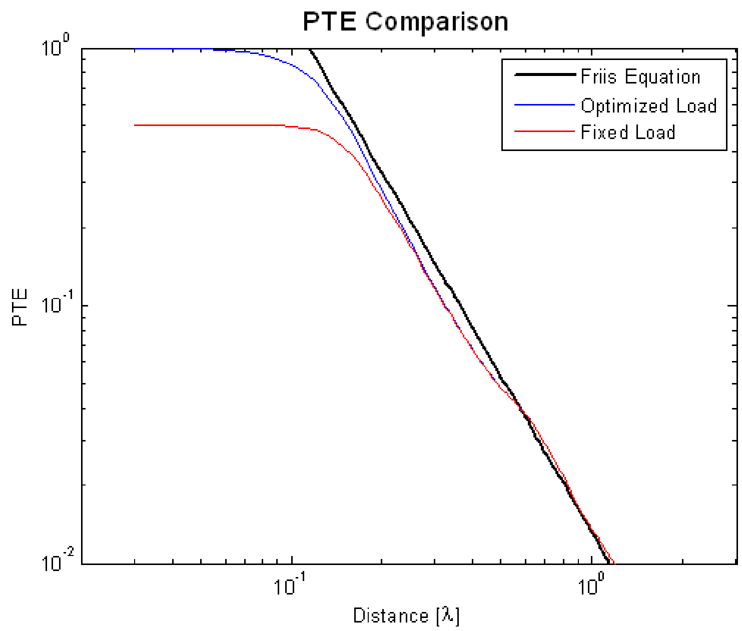

Figure 3. Single Tx single Rx PTE comparison

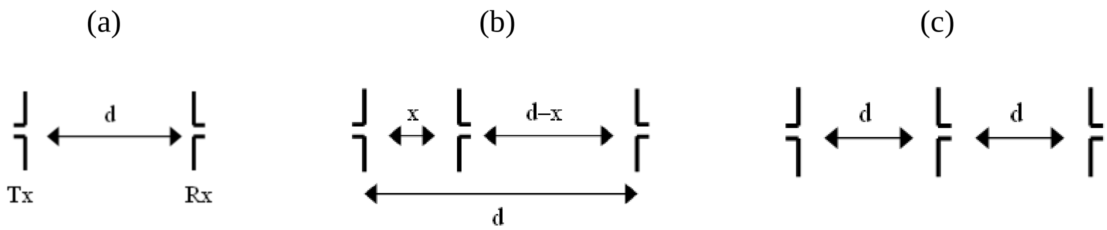

Figure 4. (a) 1Tx 1Rx configuration. (b) 3 elements with fixed total distance 'd', (c) 3 elements with the same distance 'd' from the center

transmitter or receiver adds more degrees of freedom which are distances between new elements and existing elements. To investigate the case with a simple one-dimensional (1D) plot which is the PTE versus distance curve, it is required to reduce the degrees of freedom of the problem. Two possible ways are shown in Figure 4. (b) and (c). Figure 4.

(b) illustrates that two elements are fixed at each side with a distance ‘d’ when the center element varies its position from one end to the other. Figure 4. (c) illustrates that the center element is fixed when elements at both ends change their positions with the same distance ‘d’.

2. 3. 2TX 1RX CASE AND THE REGION OF FLAT PTE VS. DISTANCE

In this section, the case of Figure 4. (b) is analyzed first with 2Tx 1Rx case. As depicted in Figure 5, when two transmitters are placed at both ends with 0.7λ distance and a single receiver is varying its position from the one end to another, we can observe a flat PTE region versus distance of approximately 21% in the middle region. There is a difference between using the fixed load and the optimized load near each end. This is because at the region close to each transmitter, the load impedances required to reach the maximum PTE is different from the value of the fixed load. As a result, the PTE is lower in the case of using the fixed load [27]. The flat region can be observed either when we use the fixed load or the optimized load at the receiver. This behavior was well investigated and proven with measurement by Yoon, et al. [27]. Figure 6 shows the NEC simulation results of FCH antennas with respect to their efficiencies. They are close to the theoretical bound [21] and the behaviors are well observed also by measurement [27].

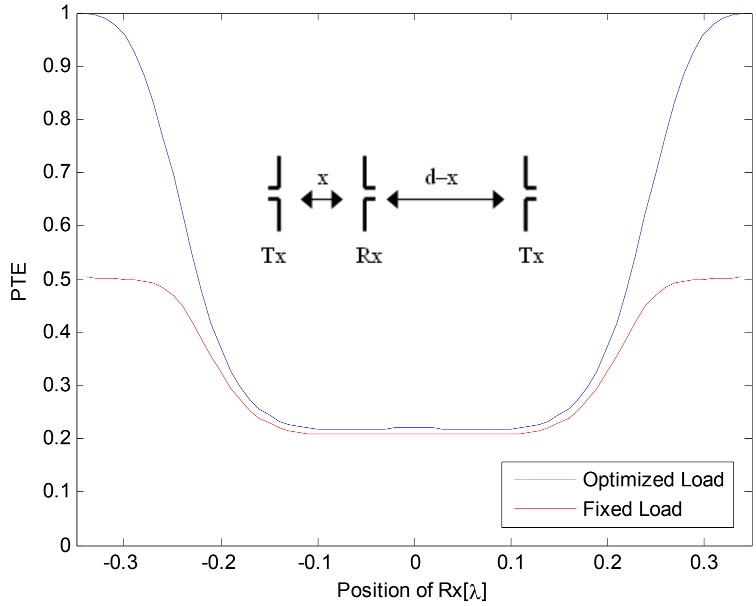

Figure 5. 2Tx 1Rx PTE comparison

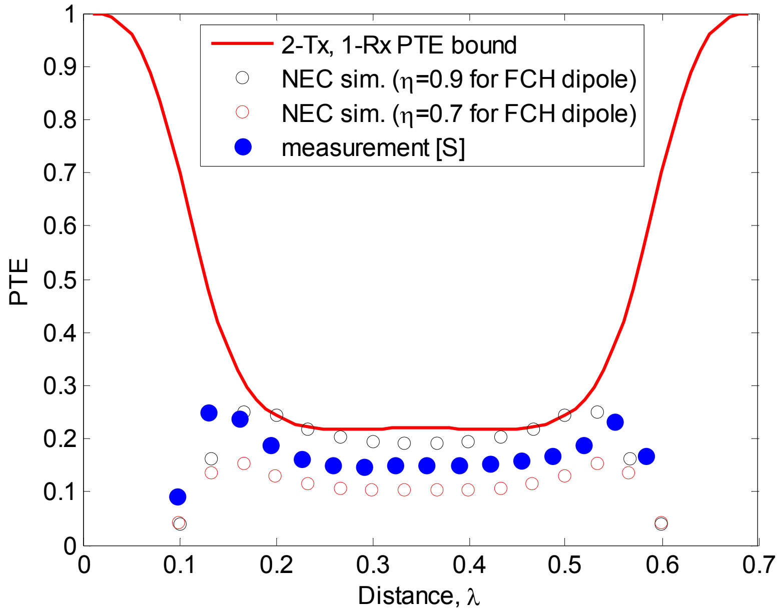

Figure 6. 2Tx 1Rx, Theoretical bound, FCH simulation, and measurement [27]

2. 4. TRANSMITTER GAIN

In this section, the case of Figure 4. (c) is analyzed for 2Tx 1Rx and 4Tx 1Rx cases. As illustrated in Figure 7. (a) for the 2Tx 1Rx case and Figure 7. (b) for the 4Tx 1Rx case, a single receiver is placed at the center and multiple transmitters are placed around the receiver. Each transmitter has a fixed distance ‘d’ to the centered receiver, and the PTE is calculated as a function of 'd'. Each transmitter should be placed as far as possible from the other transmitters. The two transmitters are placed on the opposite direction in Figure 7. (a) and each transmitter has 90 degrees of angular distance to each other in Figure 7. (b).

The result is shown in Figure 8 and we can clearly observe that there is a transmitter gain with respect to the increasing number of transmitters since the PTE curve has been shifted to the right. As we can intuitively predict, multiple transmitters generate more power so the accepted power by the receiver can be increased. However, there are larger oscillations as the number of transmitters increases. This can be explained in terms of increased mutual coupling due to reduced distance between each transmitter. The distance between each transmitter becomes closer as the number of transmitters increases.

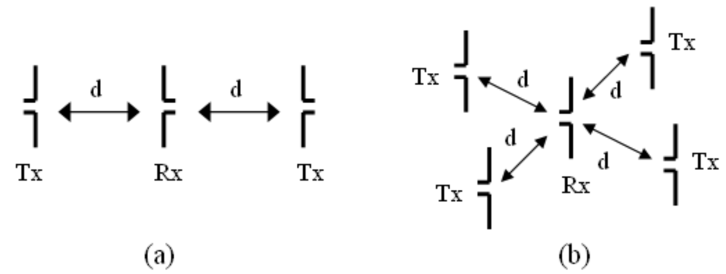

Figure 7. (a) 2Tx 1Rx, (b) 4Tx 1Rx

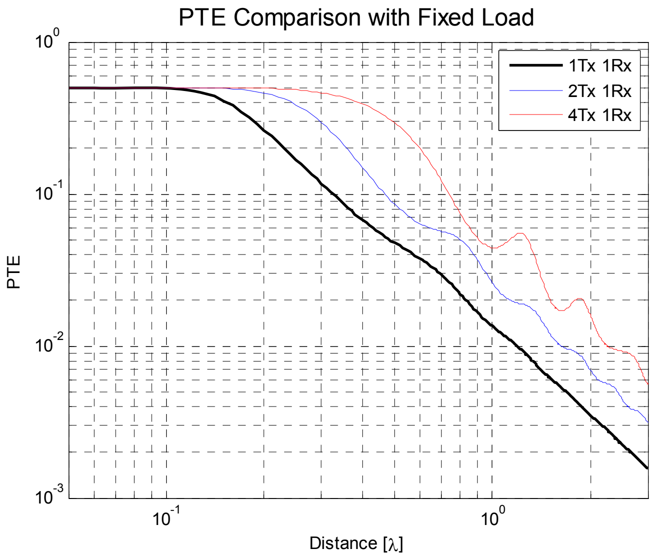

Figure 8. Transmitter gain

2. 5. SUMMARY

In this chapter, we have found that there is an improvement in the PTE, i.e., a transmitter gain, by comparing the case of multiple transmitters and a single receiver to the case of a single transmitter and a single receiver. First, the definition of the PTE and the methodology to compute it with NEC were presented in the beginning of the chapter. The simplest case, the PTE of 1Tx 1Rx, were simulated with an optimized load and a fixed load. The case of multiple transmitters and a single receiver was also investigated with two different configurations. In the first configuration, a flat PTE region versus distance was observed in the middle of two fixed transmitters. For the second configuration, we found the transmitter gain as the number of transmitters increases around a single receiver at the center.

Chapter 3 : Receiver Diversity with a Single Transmitter

This chapter presents receiver diversity in detail by investigating the case of a single transmitter and multiple receivers. The concepts of the user-wise and the system-wise PTE are introduced in the beginning. The case of the PTE versus distance is investigated first with different numbers of receivers around a single transmitter to find a receiver gain. However, degradation of PTE is also observed during the investigation of the case of the PTE versus the number of receivers. For the detailed investigation of this phenomenon, one-dimensional NEC simulation is performed with folded cylindrical helix (FCH) dipoles. Simulation is also supported by measurement. Finally, the chapter concludes with a local optimization of load impedances at receivers to find out what causes the PTE degradation.

3. 1. USER / SYSTEM VIEW

When there are N receivers deployed, PTE is separated into N+1 values since there are N individual PTEs of each receiver and an overall PTE which is simply a sum of all individual PTEs. An individual PTE can be regarded as a user-wise performance and an overall PTE as a system-wise performance. The higher an overall PTE is, the better the performance is, but this does not necessarily mean that each individual PTE is also high. It becomes very clear in the example of Table 1. Although the overall PTE of the case 2 is higher, user 2 of the case 2 suffers from extremely low PTE. As a result, the quality of service for user 2 is very poor. Therefore, for multiple receivers, we need to always consider each individual PTE.

Case	PTE of User 1	PTE of User 2	Overall PTE
1	20%	20%	40%
2	44%	1%	45%

Table 1. Example of user/system PTE difference for 2Rx case

3. 2. PTE VERSUS DISTANCE

3. 2. 1. Fixed Number of Rx

This section analyzes the case of fixed number of receivers at a constant radius from the transmitter. The configuration of the setup is shown in Figure 9. The angular separations of the receivers are maintained at a constant angle, given by (360/N), relative to each other. The PTE is plotted as a function of distance from the transmitter.

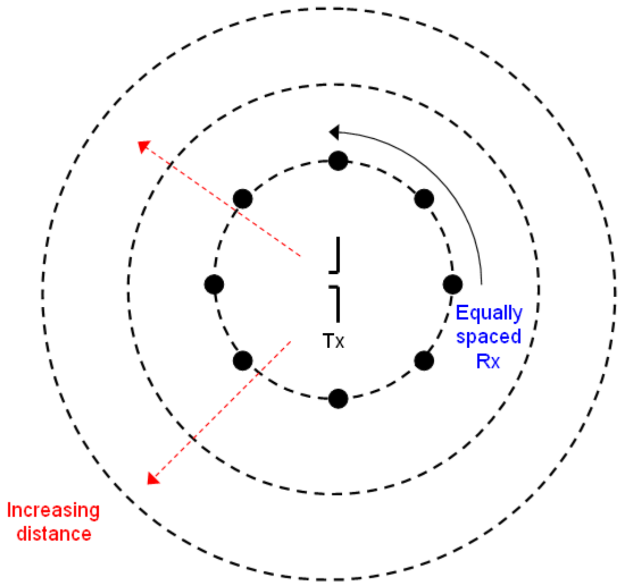

Figure 9. PTE vs. Distance configuration with fixed number of Rx

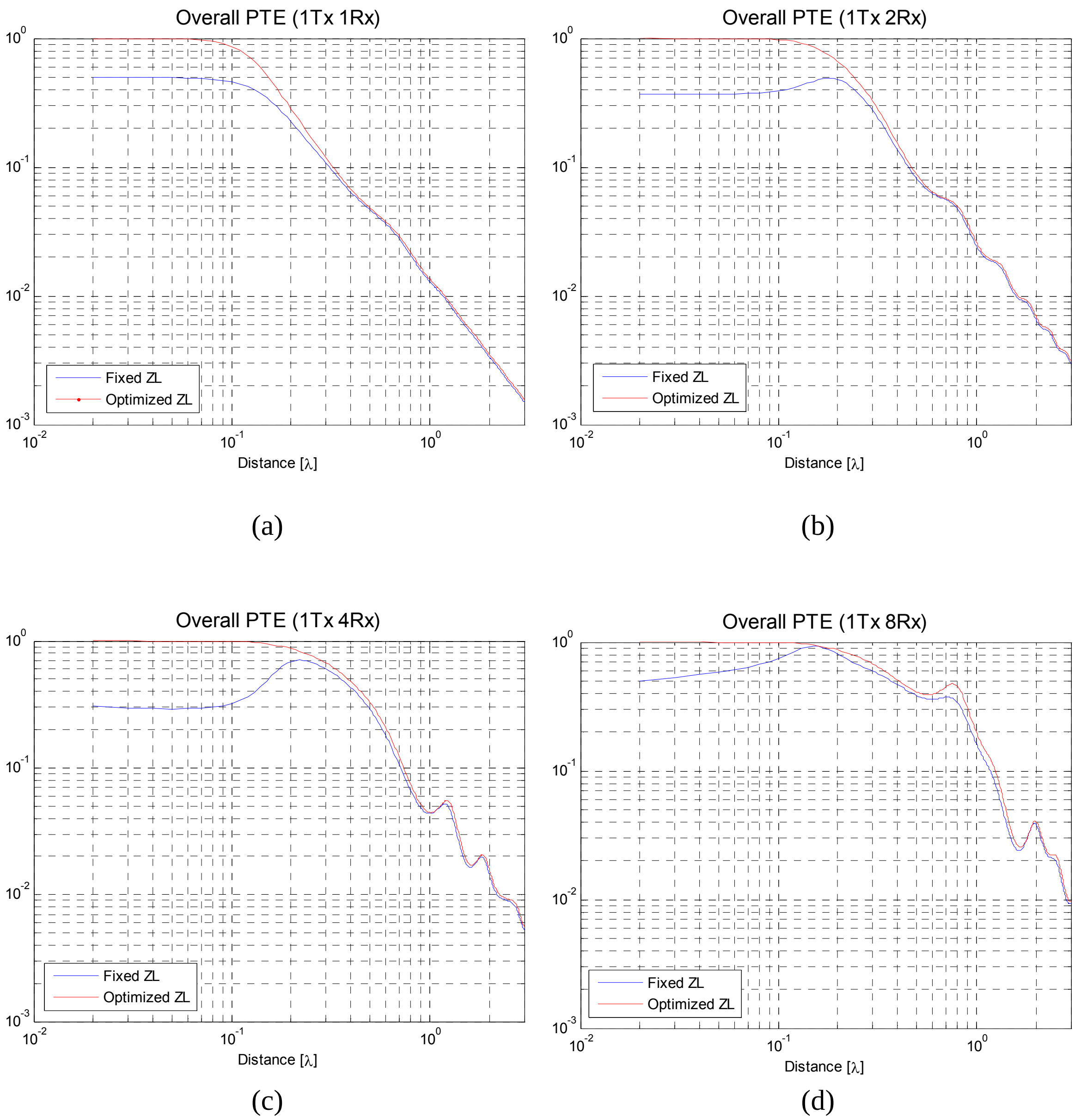

Figure 10. PTE vs. distance. Comparison between fixed load and optimized load. (a) 1Tx 1Rx, (b) 1Tx 2Rx, (c) 1Tx 4Rx, (d) 1Tx 8Rx

Figure 10 shows PTE versus distance plot of short dipoles according to the configuration of Figure 9. The distance between each receiver and the centered transmitter is increased with a fixed number of receivers, which are 1, 2, 4, and 8, for Figure 10. (a), (b), (c), and (d) respectively. The case of the PTE using a fixed load on each receiver is compared to the case of using an optimized load. Figure 10 shows that the two curves agree well beyond approximately 0.2λ from the transmitter. The fixed load impedance is matched to its complex conjugate of the antenna input impedance as in Chapter 2. Figure 11 is also the PTE versus distance plot under the same configuration, but in this case, short dipoles with fixed loads are compared to FCH dipoles with fixed loads. The load impedance of the FCH dipole is also matched to the conjugate of the antenna input impedance (the exact input impedance of FCH dipole is 49.2796 + j2.7841 [Ω] at 200.09 MHz). Although it cannot be plotted with FCH dipoles as near to the transmitter as with short dipoles due to the physical size, they agree well at other points for all 1Rx, 2Rx, 4Rx, and 8Rx cases.

From Figure 12. (a), we can observe that there is a receiver gain as the number of receivers increases. Clearly, the overall PTE curves shifted towards the right, which means each receiver accepted more power. From the aspects of users, Figure 12. (b) represents the user-wise performance, which means the overall PTE divided by the number of receivers. Besides different rippling behavior, the individual PTE curves are getting converged to the case of 1Tx 1Rx. This implies that the overall user-performance is not much different from one another when receivers are far enough from the transmitter. Figure 13 is the same plot using FCH dipoles. The plots are in good agreement with the results using short dipoles.

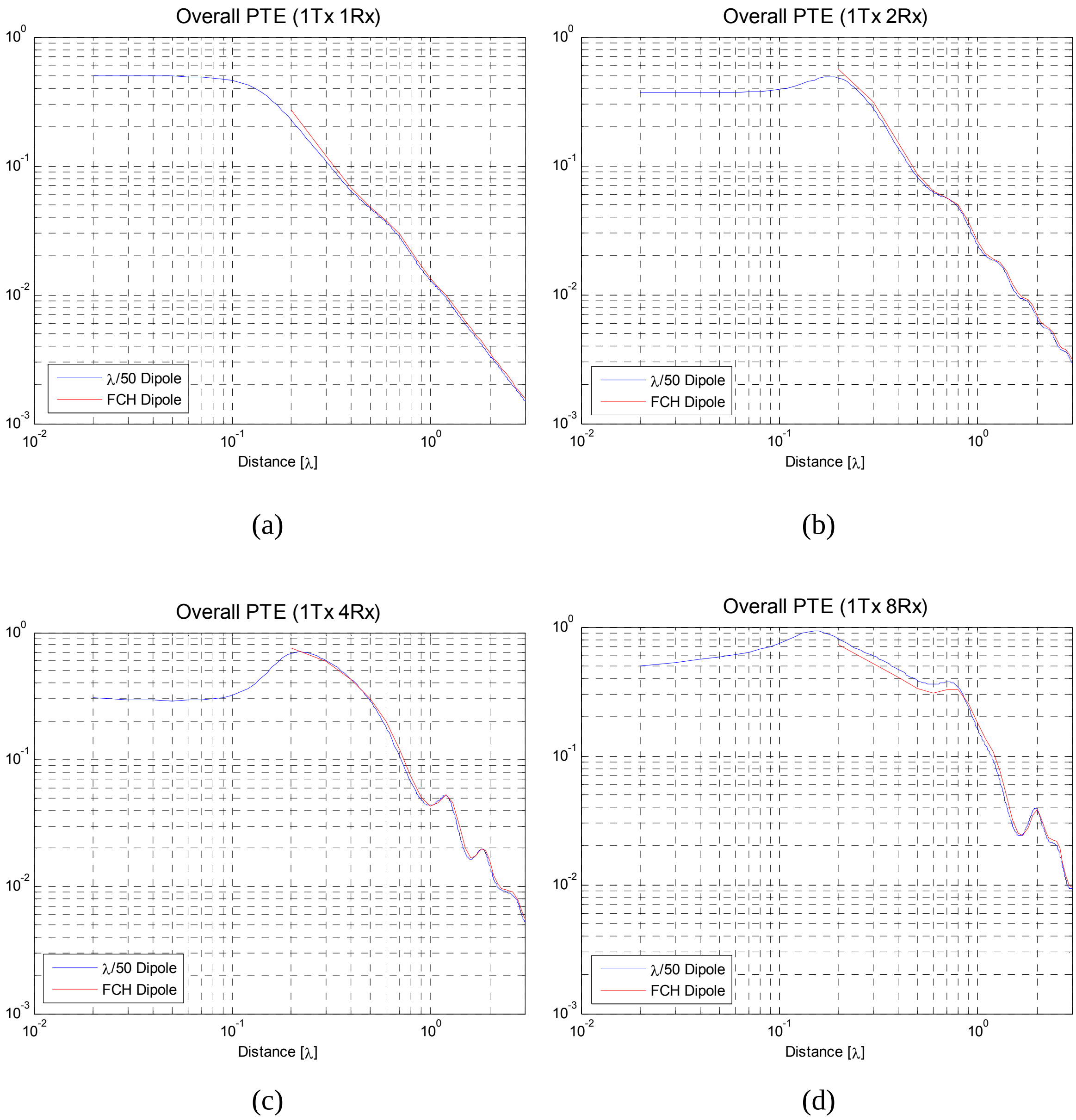

Figure 11. PTE vs. distance. Comparison between λ/50 dipole and FCH dipole both with fixed load. (a) 1Tx 1Rx, (b) 1Tx 2Rx, (c) 1Tx 4Rx, (d) 1Tx 8Rx

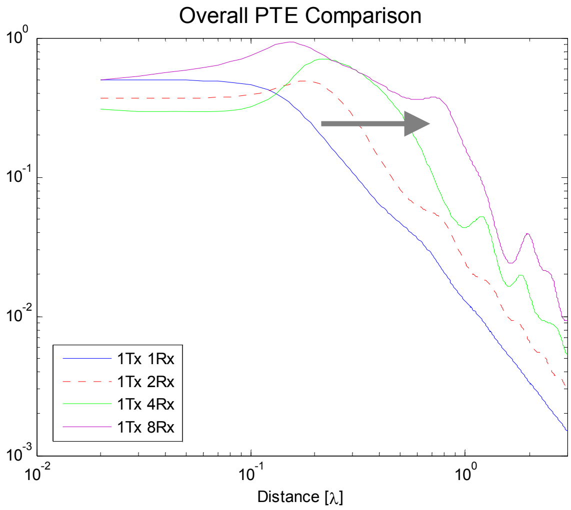

(a) Overall PTE

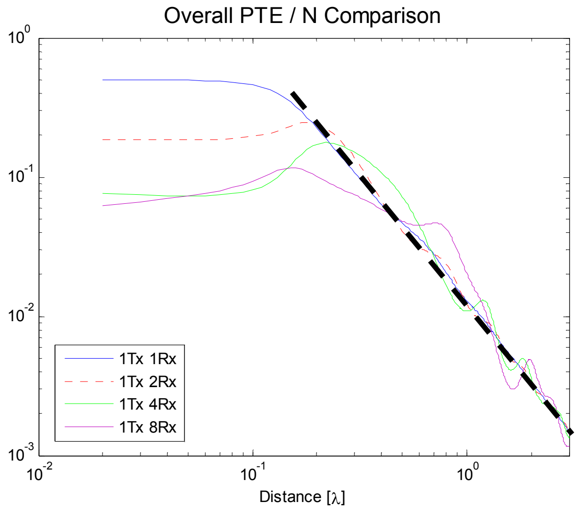

(b) Individual PTE

Figure 12. Receiver diversity gain of λ/50 dipoles

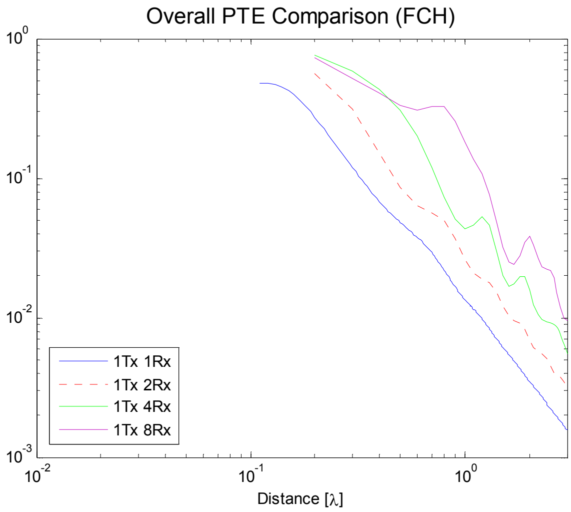

(a) Overall PTE

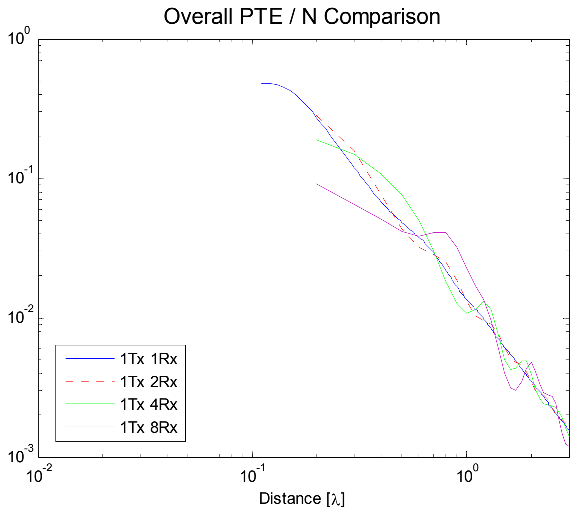

(b) Individual PTE

Figure 13. Receiver diversity gain of FCH dipoles

3. 2. 2. Fixed Distance

In this section, the PTE is calculated as a function of the number of receivers with fixed distance between a centered transmitter and each receiver around it. Receivers are to be located according to Figure 14 with the same angular distance between each receiver. Ideally, the overall PTE is expected to be increased and the individual PTE is expected to be remained the same as the number of receivers increases assuming there is no interaction such as mutual coupling between each receiver.

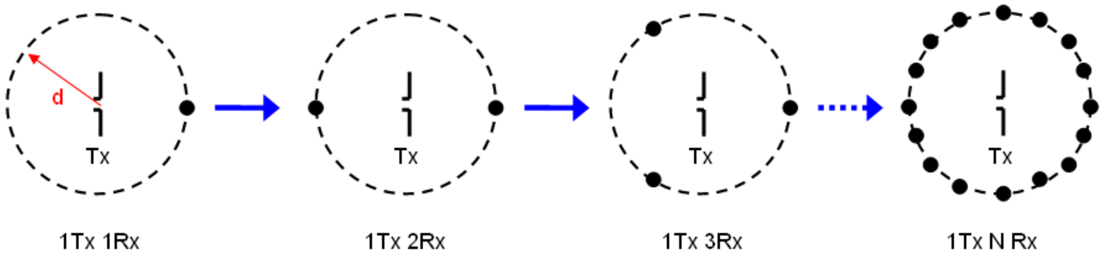

Figure 14. PTE vs. Number of Rx configuration.

However, the results in Figure 15 for short dipoles and Figure 16 for FCH dipoles do not show the expected behavior. Instead, as the number of receivers increases around the single transmitter, the individual PTE tends to drop almost to zero. This also lead to decreased overall PTE. This phenomenon is observed in Figure 15. (a), and the points of the highest overall PTE are summarized in Table 2. First, the closer receivers are to the transmitter, the higher their PTEs are. This phenomenon is observed up to the number of receivers on the second column. However, beyond the number of receivers of 7, 6, and 7 for distance of 0.2λ, 0.35λ, and 0.5λ respectively, the overall PTE starts dropping instead of increasing. This is contradictory to our ideal expectation that the overall PTE would be increased with respect to the increased number of receivers.

Distance [λ]	Number of Rx	Overall PTE
0.2	7	84.8%
0.35	6	55.6%
0.5	7	39.0%

Table 2. Points with the highest overall PTE in Figure 15. (a)

Distance [λ]	Number of Rx	Overall PTE
0.2	14	7.3%
0.35	19	8.4%
0.5	23	9.5%

Table 3. The first points of overall PTE < 10% in Figure 15. (a)

Moreover, as we take a closer look at Figure 15. (a) again, we can observe the decreasing rate of each overall PTE is different with respect to its distance from receivers to the transmitter. With an increase in the number of receivers, the onset of the point with less than 10% overall PTE for each distance is summarized in Table 3. We can find that receivers which are located nearer to the transmitter suffer from severer PTE degradation due to the increased number of receivers. With shorter distance from the transmitter, receivers have less spacing. Therefore, this can be interpreted that there is mutual coupling which prevents receivers from accepting power when two or more receivers are placed close to one another.

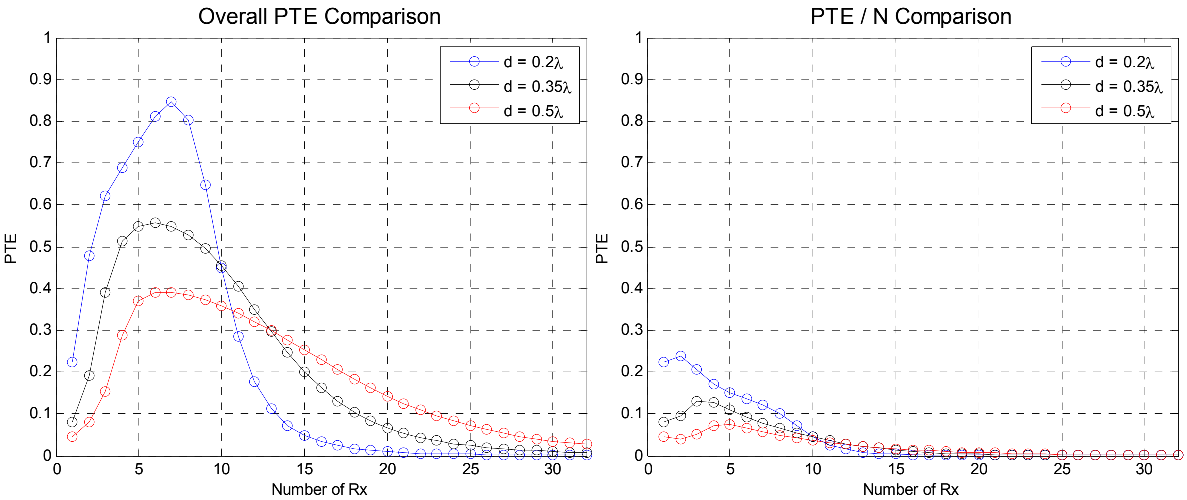

(a) Overall PTE (b) Individual PTE

Figure 15. PTE vs. Number of Rx plot for λ/50 dipoles

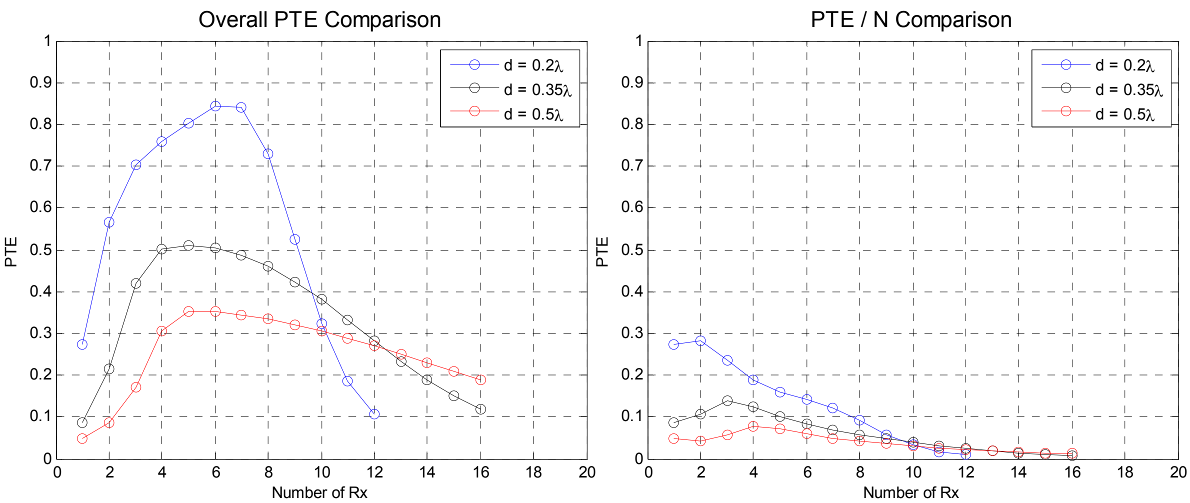

(a) Overall PTE (b) Individual PTE

Figure 16. PTE vs. Number of Rx plot for FCH dipoles

3. 3. RX COUPLING AND SINK

3. 3. 1. 2D Plot of an Overall PTE

To visually see what happens when two receivers are close together, the overall PTE is calculated on a two-dimensional plane using short dipoles. Two axes (x, y) of a 0.7λ square are divided into segments of 0.01λ length and the overall PTE is calculated with a single receiver placed at every intersection. Two transmitters are located at (-0.35λ, 0λ) and (0.35λ, 0λ). Figure 17. (a) is the resulting contour plot with steps of 10% PTE. This illustrates a flat PTE region of above 20% around a mid-point and high PTE regions near two transmitters.

For Figure 17. (b), the configuration for transmitters is the same, but one receiver (Rx1) is fixed at the center and another receiver (Rx2) is varying its position in the square. The resulting overall PTE is calculated at every intersection. Due to fixed Rx1, we can clearly see that there is degradation of the overall PTE when Rx2 is placed near Rx1. If Rx2 is located nearer than approximately 0.1λ to Rx1, the resulting overall PTE does not exceed 10%, while this PTE is more than 20% in absence of the fixed Rx1. Furthermore, when Rx2 is closer than approximately 0.06λ to Rx1, the overall PTE drops below 1%. Now it is clear that there is mutual coupling between receivers when they are closer than a certain distance. We propose to name this phenomenon as 'sink' since PTE has literally sunk when two receivers are closely located.

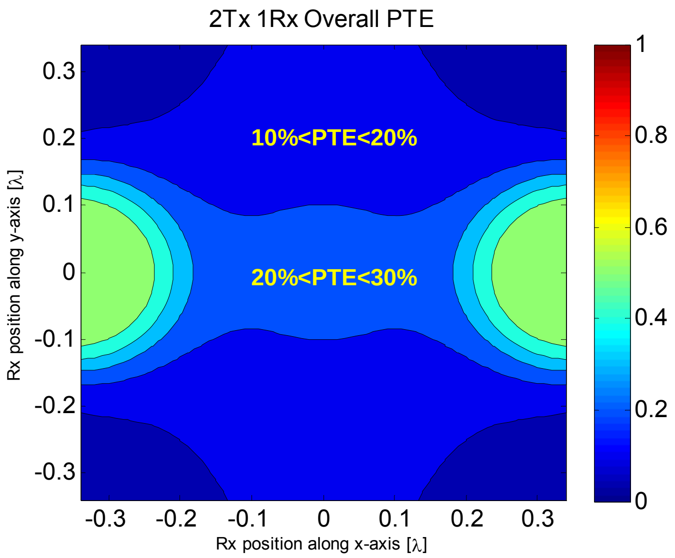

(a)

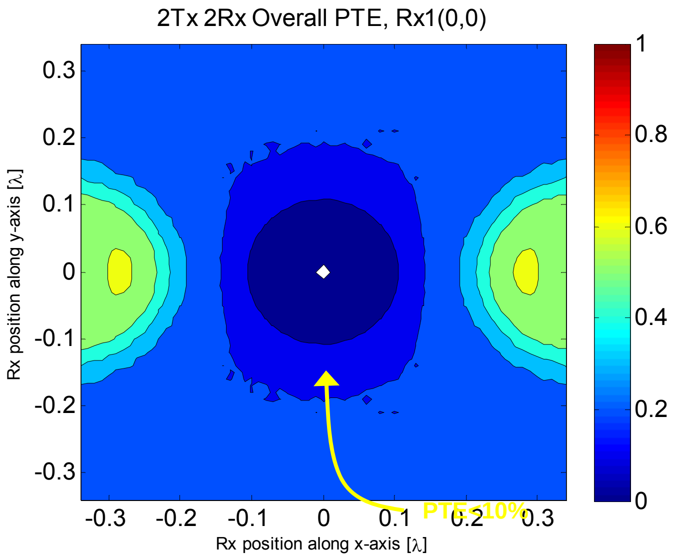

(b)

Figure 17. 2D plot of overall PTE of (a) 2Tx 1Rx, (b) 2Tx 2Rx

3. 3. 2. Simulations and measurements of Sink

To take a closer look at the sink phenomenon, one-dimensional analysis is performed with FCH dipoles to see the results more clearly from the PTE versus distance plot. The operating frequency of FCH dipoles is 200 MHz and it is loaded with copper (σ =5.96x10^7). The simulation setup is illustrated in Figure 18. The transmitter is fixed at the origin and Rx1 is fixed at 0.2922λ from the transmitter. Distance between the transmitter and Rx1 is determined for consistency with the measurement since 0.2922λ is 45cm at 194.8 MHz. Rx2 varies its position from 0λ to 1λ. Due to the physical size of an FCH dipole which is about 10.2cm in diameter, the closest distance between the transmitter and Rx1 is set to 12cm in measurement and 0.07λ in simulation. The fixed load impedance has been chosen to be 50 + j0 [Ω] to have consistency with 50Ω termination in measurement.

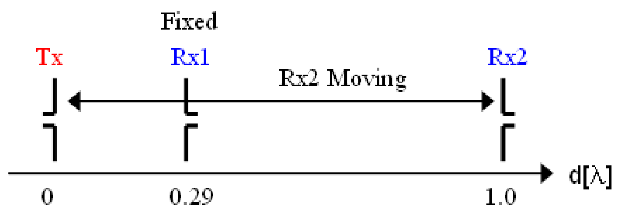

Figure 18. Configuration of ‘sink’ simulation

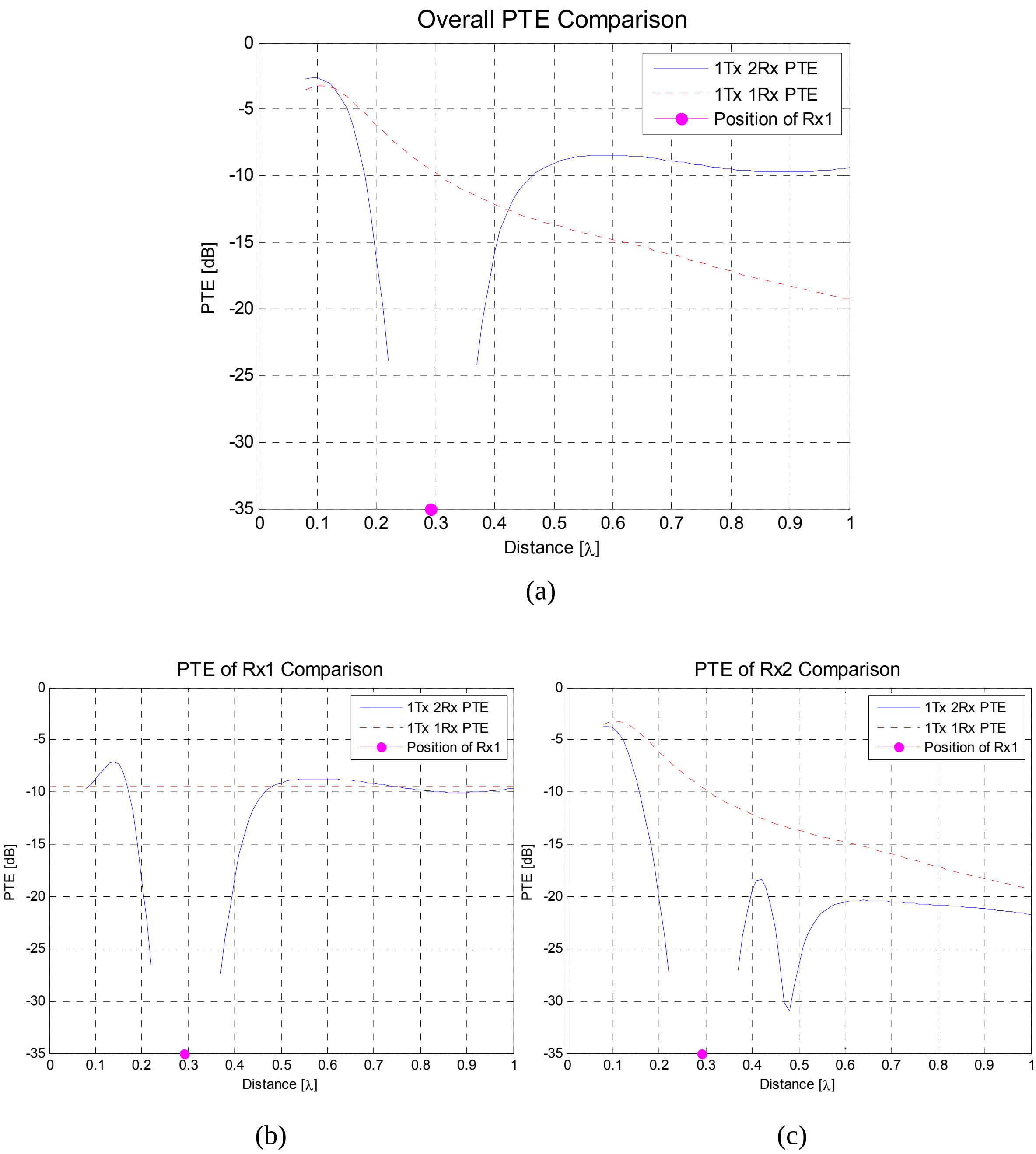

Figure 19. 1D simulation of sink. (a) Overall PTE, (b) Individual PTE of Rx1, (c) Individual PTE of Rx2

Figure 19 is the results of the simulation in which the PTE is plotted on dB scale as a function of distance from the transmitter. Figure 19. (a) is the overall PTE, which is the sum of PTE of Rx1 and Rx2. The sink phenomenon is clearly observed around fixed Rx1. Compared to the PTE of 1Tx 1Rx case, in the region from distance of 0.14λ to 0.42λ, the overall PTE is lower. This is about 0.15λ to the left of Rx1 and 0.13λ to the right. In Figure 19. (b), the PTE of Rx1 with respect to the position of Rx2, the sink phenomenon can be observed compared to -9.5dB (red dotted line), which is the PTE value of Rx1 at 0.2922λ when there is no other receivers. In Figure 19. (c), the PTE curve of Rx2 also clearly shows the sink phenomenon compared to the PTE of 1Tx 1Rx case.

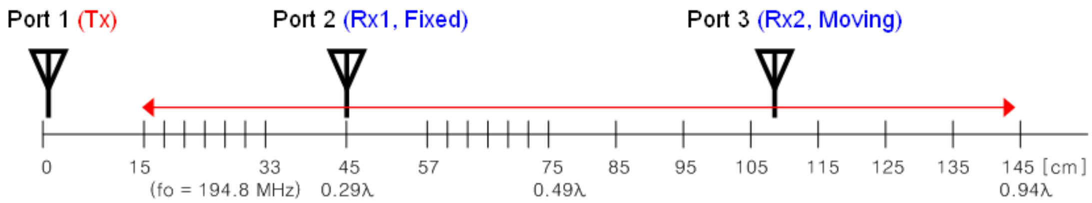

Figure 20. Measurement setup

Figure 21. Indoor measurement

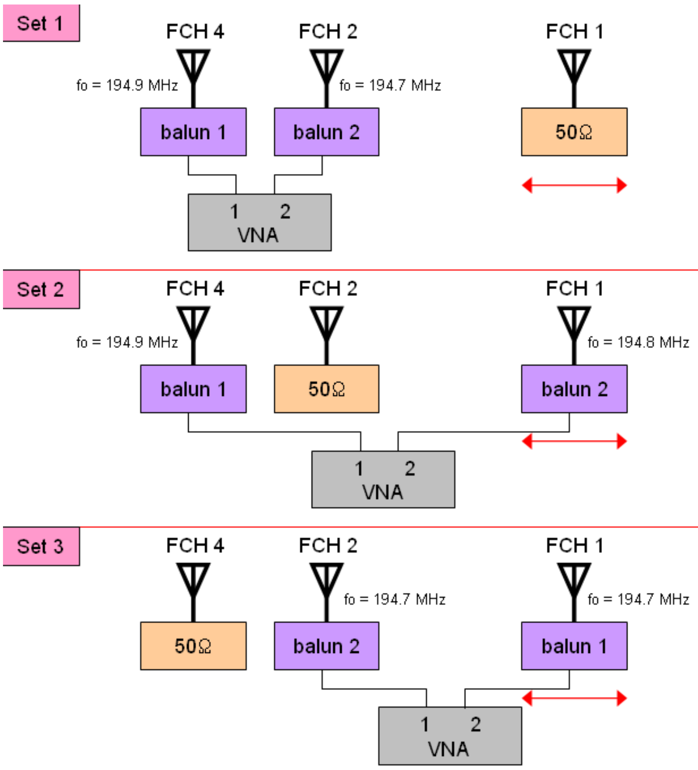

$$\begin{pmatrix} S_{11} & S_{12} \\ S_{21} & S_{22} \end{pmatrix} \Rightarrow \begin{pmatrix} S_{11} & S_{12} & \mathrm{N/A} \\ S_{21} & S_{22} & \mathrm{N/A} \\ \mathrm{N/A} & \mathrm{N/A} & \mathrm{N/A} \end{pmatrix}$$

$$\begin{pmatrix} S_{11} & S_{12} \\ S_{21} & S_{22} \end{pmatrix} \Rightarrow \begin{pmatrix} S_{11} & \mathrm{N/A} & S_{12} \\ \mathrm{N/A} & \mathrm{N/A} & \mathrm{N/A} \\ S_{21} & \mathrm{N/A} & S_{22} \end{pmatrix}$$

$$\begin{pmatrix} S_{11} & S_{12} \\ S_{21} & S_{22} \end{pmatrix} \Rightarrow \begin{pmatrix} \mathrm{N/A} & \mathrm{N/A} & \mathrm{N/A} \\ \mathrm{N/A} & S_{11} & S_{12} \\ \mathrm{N/A} & S_{21} & S_{22} \end{pmatrix}$$

Figure 22. Constitution of 3x3 S-matrix

Figure 20 is the measurement setup. Finer measurement points have been set near fixed Rx1 from 15cm to 75cm with 3cm increment, and 10cm increment has been applied from 75cm to 145cm. Since the measurement was done using 2-port Vector Network Analyzer (VNA), the measurement was needed to be divided into 3 sets as illustrated in Figure 22. At each set, two FCH dipoles were connected to the VNA and the remaining dipole was terminated with 50Ω load. Data of 2x2 S-matrix were collected by the VNA and three 2x2 S-matrices constituted a whole 3x3 S-matrix. Since dipoles were used in measurements, a differential signal of a dipole needed to be transformed to a single-ended signal and this is done using a balun in the same way as had been done in [27].

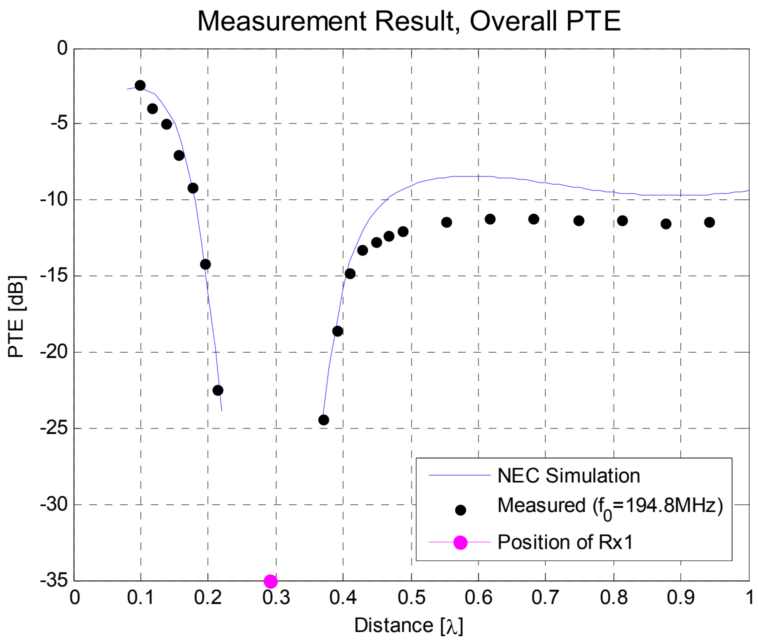

(a)

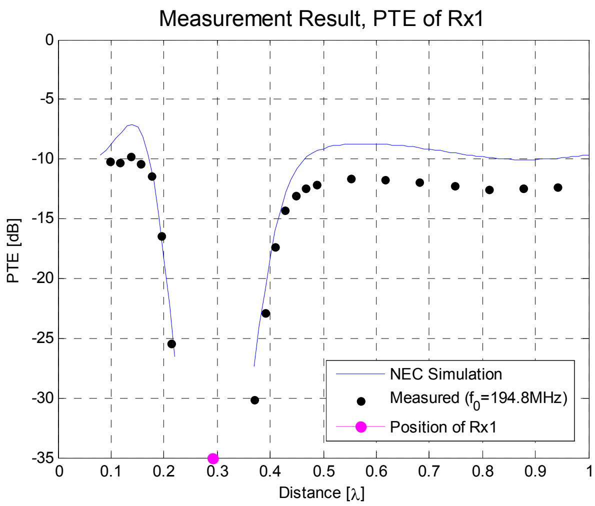

(b)

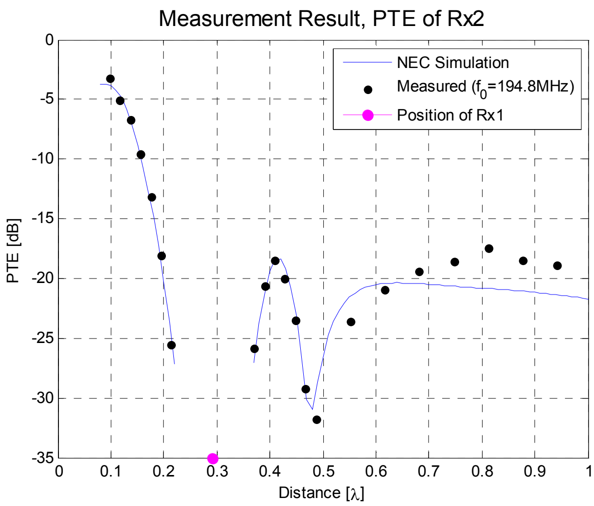

(c)

Figure 23. Measurement results. (a) Overall PTE, (b) Individual PTE of Rx1, (c) Individual PTE of Rx2

The resonance frequency of FCH dipoles differ very slightly depending on which balun and which antenna have been used as depicted in Figure 22. The representative frequency for plotting the result has been chosen to be 194.8 MHz. With complete set of S-parameters, the PTE is calculated as Eq. (5).

$$PTE = \frac{|S_{21}|^2 + |S_{31}|^2}{1 - |S_{11}|^2} \tag{5}$$

The measurement result is shown in Figure 23. This agrees well with the NEC simulation data of Figure 19, which successfully supports the sink phenomenon.

3. 3. 3. Sink due to Mismatched Load

In this section, a possible explanation for a sink is sought. For the case of a single transmitter and a single receiver, it has been already observed in Figure 3 in Chapter 2 that the PTE using an optimized load and a fixed load do not have much difference beyond approximately 0.2λ from the transmitter. Figure 3, illustrating an optimized PTE, is depicted again as Figure 24. (a) for convenience. Figure 24. (b) is its corresponding optimized load impedance. Within 0.2λ from the transmitter, the PTE starts to differ with respect to its load impedance as shown in Figure 24. (b). This leads us to assume that the PTE drop in the sink region is due to the fact that load impedance for the maximum PTE is different from the fixed value when two receivers are close.

To prove this, a local optimization has been performed under the same configuration as Figure 18 with FCH dipoles. At every position of Rx2, a Y matrix has been generated by the NEC simulation and the number 1, 2 and 3 are assigned to the transmitter, Rx1, and Rx2 respectively. Eq. (5) describes how Y parameters are related to voltages and currents where $V_{1\sim3}$ and $I_{1\sim3}$ are terminal voltages and current. V_1 was set

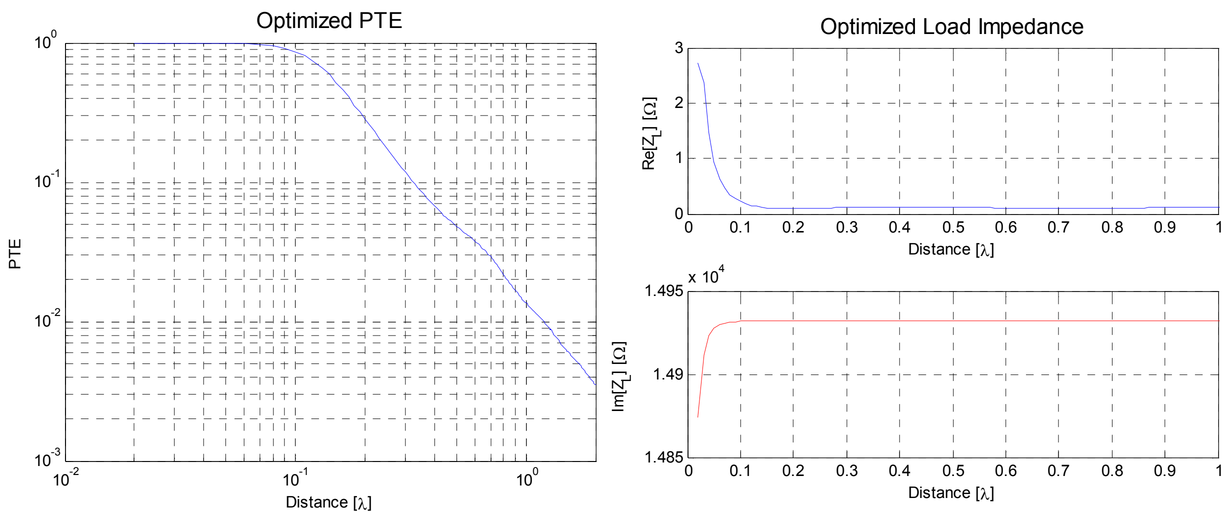

Figure 24. 1Tx 1Rx optimized PTE revisited. (a) Optimized PTE, (b) Corresponding optimized load impedance

as 1 [V] since the transmitter is excited with 1+j0 in the NEC and V_2 and V_3 are equal to $-I_2Z_L$ and $-I_3Z_L$ respectively, where Z_L is the complex load impedance at each receiver. $I_{1\sim3}$ are obtained from the result of NEC simulation.

$$\begin{pmatrix} Y_{11} & Y_{12} & Y_{13} \\ Y_{21} & Y_{22} & Y_{23} \\ Y_{31} & Y_{32} & Y_{33} \end{pmatrix} \begin{pmatrix} 1 \\ -I_2Z_L \\ -I_3Z_L \end{pmatrix} = \begin{pmatrix} I_1 \\ I_2 \\ I_3 \end{pmatrix} \quad \Rightarrow \quad \begin{pmatrix} 1 & Y_{12}Z_L & Y_{13}Z_L \\ 0 & 1+Y_{22}Z_L & Y_{23}Z_L \\ 0 & Y_{32}Z_L & 1+Y_{33}Z_L \end{pmatrix} \begin{pmatrix} I_1 \\ I_2 \\ I_3 \end{pmatrix} = \begin{pmatrix} Y_{11} \\ Y_{21} \\ Y_{31} \end{pmatrix} \qquad (6)$$

In Eq. (6), 3 unknown currents are calculated from the input of two variables which are the real and imaginary part of Z_L. To make the optimization simpler, the same load impedances have been applied to both two receivers. The starting point for Rx2 of local optimization is 1.0λ with a seed value of the complex conjugate of the input impedance of the FCH dipole. Rx2 varies its position towards the transmitter with -0.001λ step. At each position, the resulting optimized load impedance has been used for the seed value of the next location. Although this is limited optimization with the same load impedance for each receiver and with only a single seed value, it is sufficient to prove that a change in the load impedance yields better PTE even when two receivers are in the sink region. The results are depicted in Figure 25. (a). It shows that although there is a little degradation in the PTE, it is much better compared to when there is a sink region. From Figure 25. (b) and (c), it is observed that the load impedance changed dramatically around fixed Rx1. This explains why the fixed load has resulted in such a low PTE when receivers are in the sink region. Figure 26 is the comparison between the optimized load and the fixed one, and clearly shows the difference between the two.

3. 4. SUMMARY

In this chapter, receiver diversity has been investigated in detail. First, the concept of the individual PTE was separated from the overall PTE to represent the user-wise performance. As in the case of multiple transmitters and a single receiver in Chapter 2, the PTE versus distance plot of the case of a single transmitter and multiple receivers showed a receiver gain. However, from the simulations of the PTE versus the number of receivers at fixed distance, a degradation in the PTE was found due to mutual coupling when two or more receivers are close together. This was termed as a sink phenomenon and this was supported by simulation and measurement. As a further investigation, a mismatched load impedance of receivers was postulated as the cause of the sink phenomenon. This was proven by achieving higher PTE using the load impedance obtained from a local search.

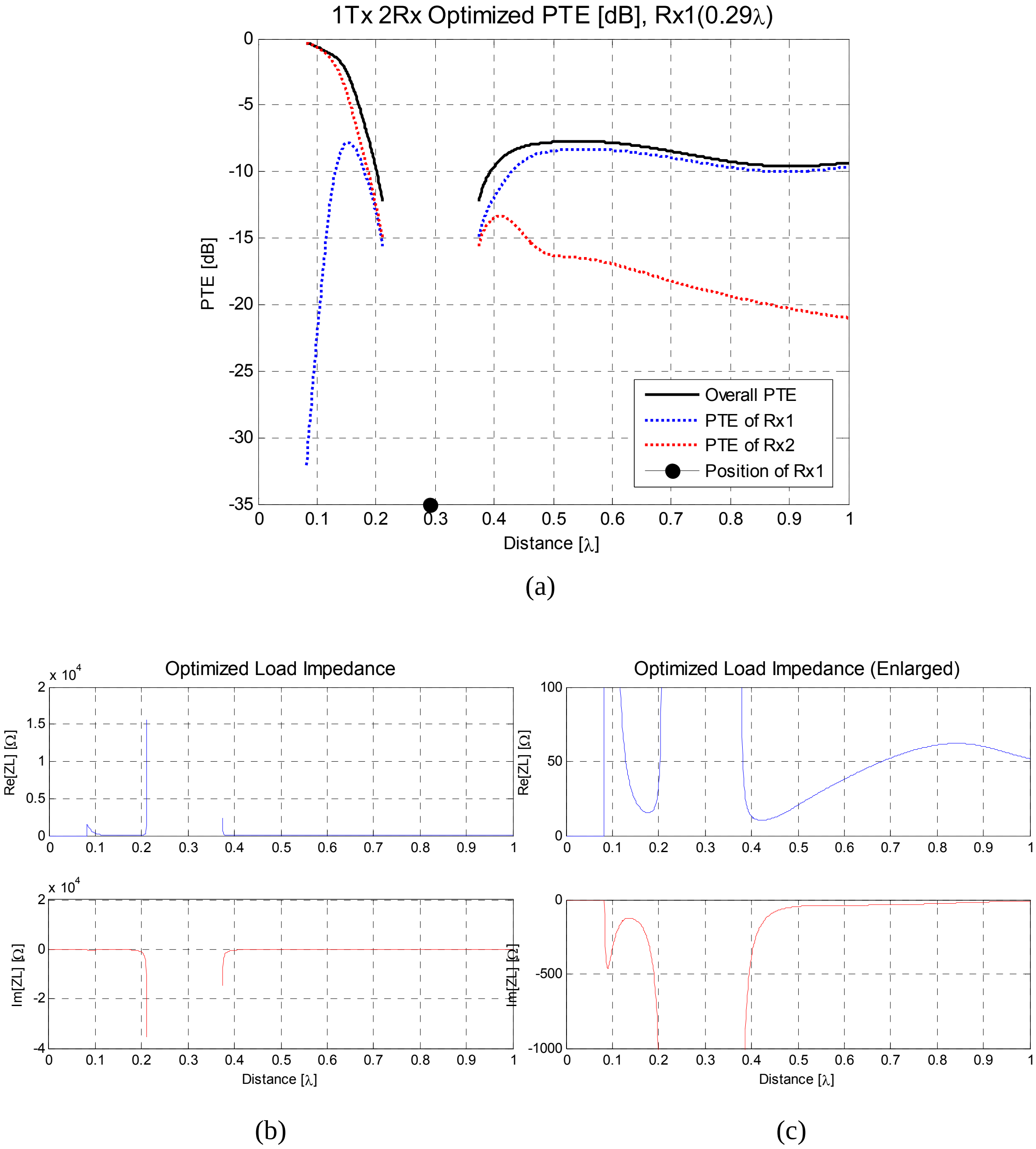

Figure 25. Local optimization results. (a) PTE, (b) and (c) Optimized Z_L

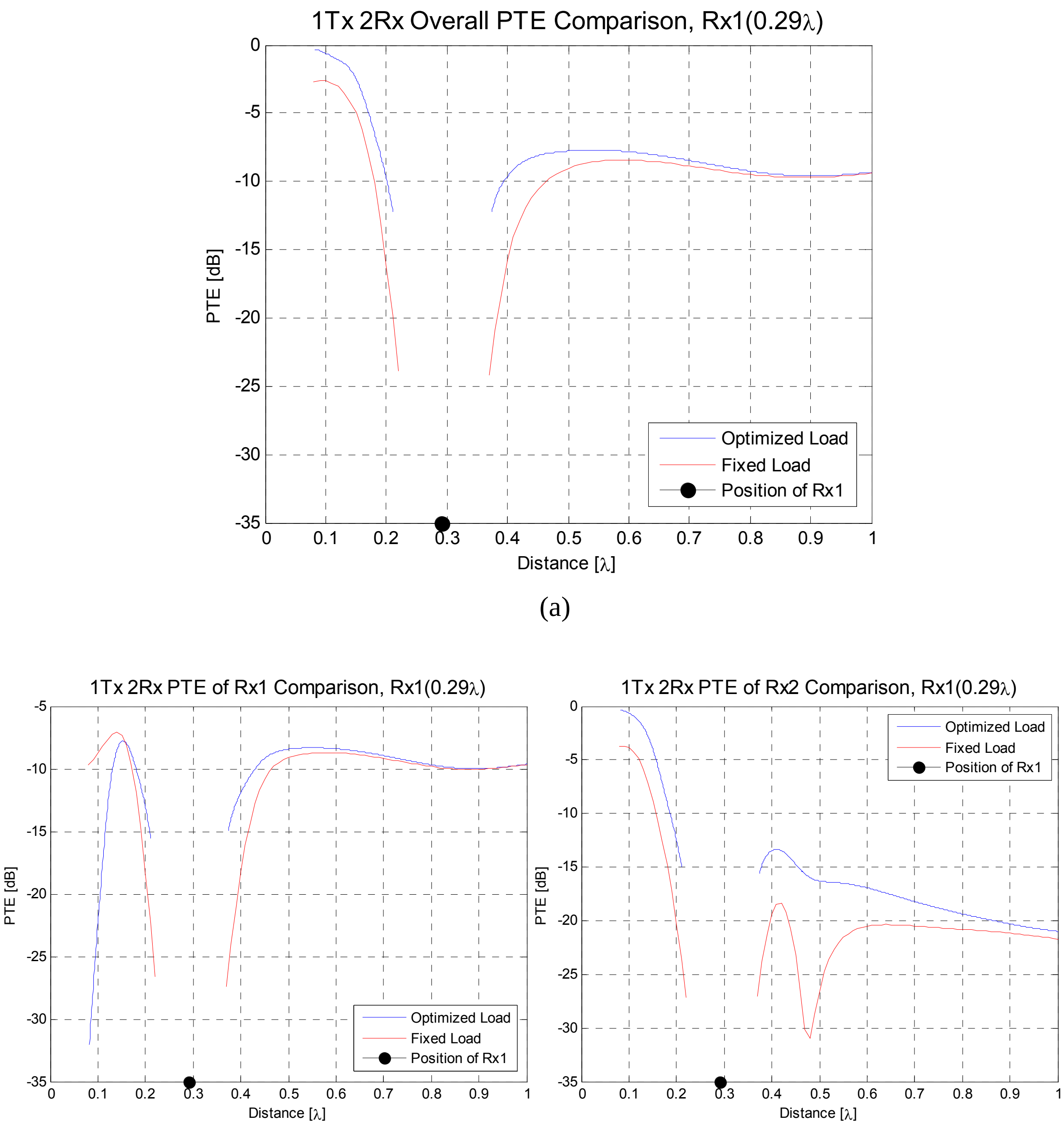

(a)

(b) (c)

Figure 26. PTE comparison between using optimized and fixed load for FCH dipoles. (a) Overall PTE (b) Individual PTE of Rx1 (c) Individual PTE of Rx2

Chapter 4 : Monte-Carlo Simulations under General Situations

An approach using Monte-Carlo simulations to investigate the transmitter and receiver diversity is proposed in this chapter. Previously we have considered only constrained situations such as fixed distance between each transmitter and receiver. As a result, we have not been able to consider all the possible locations of transmitters or receivers. The result was a one-dimensional PTE versus distance plot, which is easily understood and intuitive. The advantages of using Monte-Carlo simulations are that all possible locations of multiple receivers are considered, and it provides statistical results for any given situation. The results from previous chapters, such as diversity gain and the sink phenomenon, can also be found using Monte-Carlo simulations.

The first section of this chapter introduces a methodology of the Monte-Carlo simulation. A probability density function (PDF) and a cumulative distribution function (CDF) are introduced as ways to interpret more general situations. In the second section, the case of a single transmitter and a single receiver is explored using Monte-Carlo simulation to provide an example to interpret the PDF and CDF curves. In the third section, the comparison between a far-field CDF and a near-field CDF is provided with a case of 2Tx 1Rx. As a result, a sink phenomenon is also observed in the CDF curve in the near-field case. To overcome the sink phenomenon, constraints for receiver positions are proposed in the fourth section. Finally, with the constraints applied, the transmitter and receiver gains are fully investigated.

4. 1. DESCRIPTION AND METHODOLOGY OF MONTE-CARLO SIMULATION

In this chapter, since a dipole antenna has an omnidirectional radiation pattern along its azimuth plane only two-dimensional situations are considered. For Monte-Carlo simulation, short dipoles are simulated in NEC. The operating frequency has been set to 30 MHz because the wavelength at this frequency is feasible for real-world applications. For example, in Figure 17. (a), the distance from one of the transmitters to the mid-point of the flat region is 0.35λ. For 200 MHz this distance is about 0.5m, but for 30 MHz it is about 3.5m. Therefore, we can imagine a room environment from Figure 17. (a), and each point represents the PTE provided to a user at that spot. Changing the frequency from 200 MHz to 30 MHz does not make any significant change in the results of NEC simulations.

Monte-Carlo simulation is set up as follows. First, the geometry of interest is defined, for example, a circle or a square. This is a boundary for random receiver position. Transmitters are fixed by a specified rule throughout the whole simulation and this will be discussed again in section 4. 5. Second, random numbers are generated with uniform distribution to represent a Cartesian coordinate of each receiver location (x, y). If (x, y) is out of the region of interest, it is discarded. The fixed transmitters and randomly placed receivers constitute one set of a single execution of NEC. Short dipoles are used for the NEC simulation and the load impedance of receivers is fixed to 0.110596 – j0.102534E+05[Ω] which is the complex conjugate of the input impedance of a short dipole at 30 MHz. For each execution, overall and individual PTEs are calculated in the same way as the previous chapters.

The calculation process is repeated for N times. After N iterations, the probability density function (PDF) and cumulative distribution function (CDF) are obtained for the overall PTE and the individual PTE. These two functions will be a key factor to understand effects of multiple transmitters and receivers when one-dimensional PTE versus distance plot is not provided. Additionally, the average of N overall PTEs and N individual PTEs are also used as indices which represent performances of the system. N has been determined by a convergence test and it has been observed that N=10,000 is sufficient to reach stable curves of PTE with error approximately less than 0.5% of the average PTE.

4. 2. SINGLE TX SINGLE RX CASE AND IDEAL TX/RX GAIN

The result of the Monte-Carlo simulation of 1Tx 1Rx case is depicted in Figure 27. At this time, the PDF and CDF curves are the same for the overall PTE and the individual PTE since there is only one receiver. The region of interest is a circle of 0.35λ radius and a single transmitter is placed at the center. In Figure 27. (a), the PDF has two peaks. The first peak shows a 7% probability of having a PTE around 10% and the second peak shows 3% probability of having a PTE around 50%. This can be compared to Figure 28, which describes the PTE of every point in the region of interest. In Figure 28, in the center, the region of PTE from 40% to 50% is relatively bigger than other area, which represents the peak at 50% PTE in Figure 27. (a). The region of PTE from 10% to 20% is also relatively bigger, and due to truncation of the geometry of interest, the region of PTE less than 10% is very narrow. This causes the peak at 10% PTE in Figure 27. (a). These two peaks in the PDF curve correspond to two sharp rises in the CDF curve in Figure 27. (b). From the understanding of a PTE in a CDF curve, we can imagine how the transmitter and receiver diversity gain will look in terms of a CDF curve. For the overall PTE, if there is an improvement in the PTE by adding more transmitters or receivers, a CDF curve will shift to the right, which means there is a statistically higher probability of

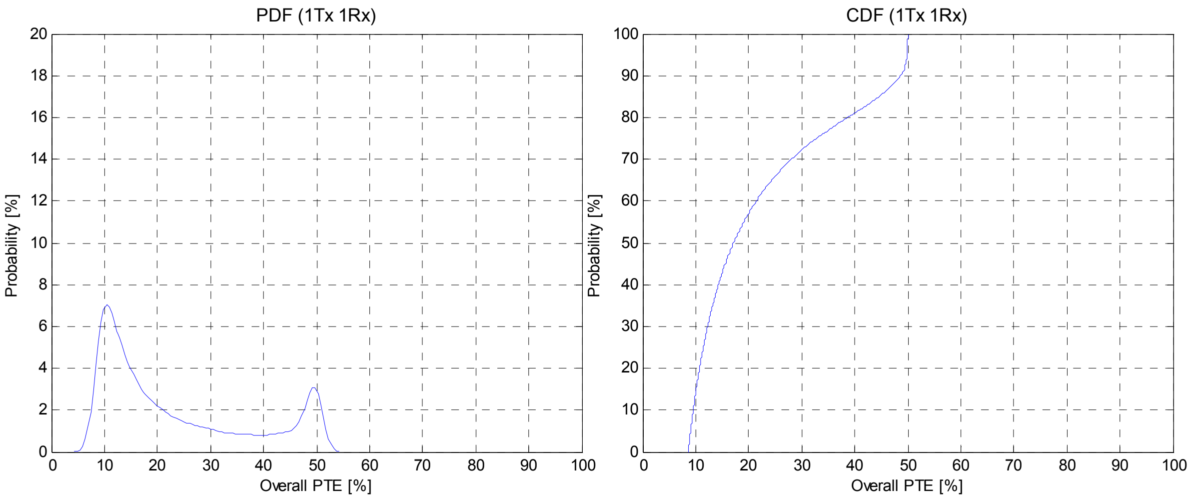

Figure 27. (a) PDF and (b) CDF of PTE of 1Tx 1Rx case after 10,000 executions of NEC simulation with random Rx placement

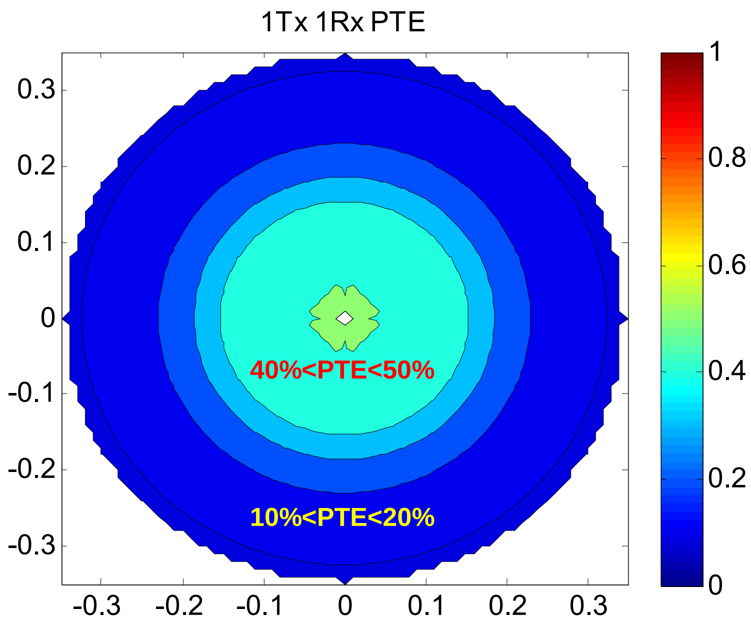

Figure 28. 2D plot of 1Tx 1Rx PTE, a circle of radius 0.35λ, Tx at origin

getting a higher PTE. This is the system-wise gain. Individual PTE is not expected to rise when there are more receivers, because a receiver is only a power consumer and does not provide additional power to other receivers. Therefore, from a user's point of view, the ideal behavior of a CDF curve is to stay the same regardless of the number of receivers. However, if there is any mutual coupling as observed in Chapter 3, the CDF of individual PTE will be shifted to the left, which indicates degradation of the user-wise PTE.

4. 3. NEAR / FAR FIELD COMPARISON

Figure 29 is the CDF curve of the overall and the individual PTE for two receivers placed randomly in a circle of radius 2.0λ and a single transmitter placed in the center. The overall PTE is depicted in Figure 29. (a) and the CDF curve has been shifted to the right which means there is a receiver gain in the overall PTE. For Figure 29. (b), the individual PTE for 1Rx and 2Rx cases are almost the same which meets the ideal expectation in the previous section. A radius of 2.0λ is enough to be in the far-field of the transmitter, and the chance of two receivers placing close together is not relatively high. Therefore, it behaves as if there is no mutual coupling. However, when the region of interest is smaller, mutual coupling starts to appear between receivers and the resulting CDF becomes different. The overall PTE does not increase as much as expected, and the individual PTE decreases due to the mutual coupling.

In Figure 30. (a), the overall PTE looks similar to the ideal behavior since the CDF curve is shifted to the right. However, focusing on the bottom of the CDF (red circle), it can be seen that the probability of 2Rx PTE having almost 0% is increased compared to 1Rx PTE. This is a the result of the increased probability of two randomly placed receivers being located close enough for mutual coupling due to the reduced size of the region. This causes low PTE, and this region of reduced PTE indicates the sink phenomenon. Figure 30. (b) describes the individual PTE under the same situation. The sink region can be also observed in the CDF curve from the increased region of low PTE. Furthermore, the individual PTE is shifted to the left which indicates PTE degradation due to mutual coupling. There is a tradeoff between the sink phenomenon and the PTE. If the region of interest is large enough, a sink phenomenon rarely occurs but the resulting PTE is too low. However, if the region of interest is small, the resulting PTE is relatively high, but it suffers from mutual coupling and the sink phenomenon.

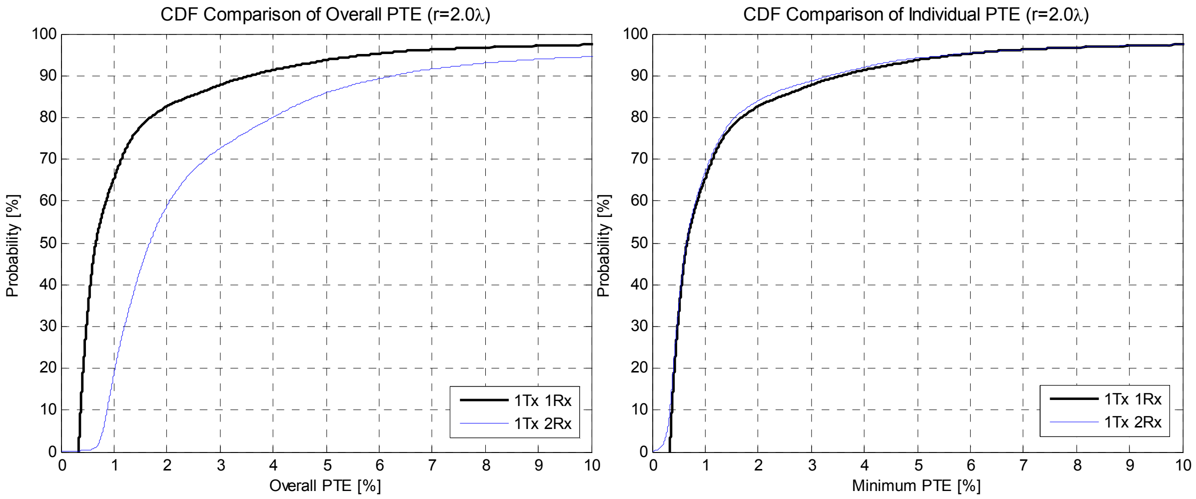

Figure 29. 1Rx and 2Rx CDF comparison of overall PTE, Radius = 2.0λ, Tx at origin

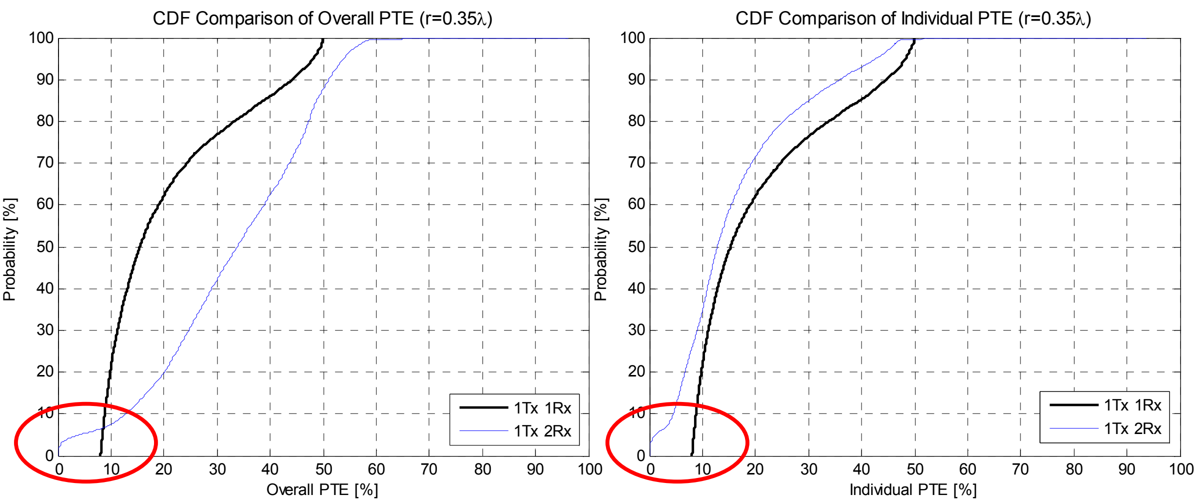

Figure 30. 1Rx and 2Rx CDF comparison of overall PTE, Radius = 0.35λ, Tx at origin

4. 4. CONSTRAINTS OF MONTE-CARLO SIMULATION

Previously, we have discussed the sink phenomenon which prevents a receiver from accepting power due to mutual coupling. From Figure 17. (b), it seems that the sink region has a size of approximately 0.1λ radius around Rx1. Therefore, to prevent the sink phenomenon, constraints are applied to the positions of receivers as depicted in Figure 31. If Rx2 is to be randomly located in a circle around Rx1 within a radius of guard spacing (GS), the random position is discarded and Rx2 is re-located until it is both inside the region of interest and out of the region of guard spacing. If a guard angle (GA) is applied to Rx1, Rx2 cannot be located inside the guard angle in Figure 31.

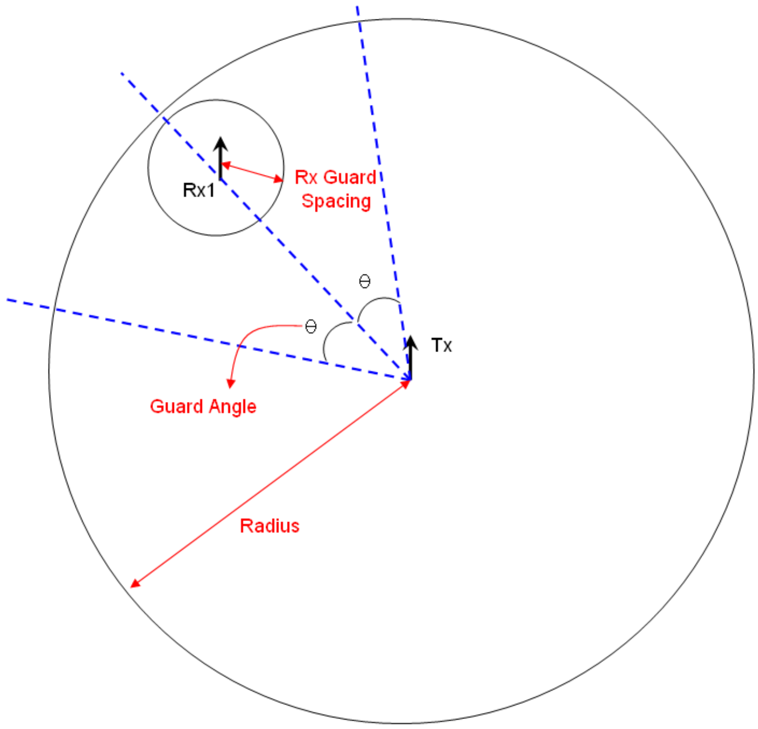

Figure 31. Constraints for Rx placement

Figure 32 and Figure 33 are the resulting CDF curves for the overall PTE and the individual PTE respectively, for 1Tx 2Rx case. Both two CDF curves are shifted to the right in the order of no constraint, guard spacing, and guard angle. This implies that as constraints are applied, the overall PTE has higher values and degradation of the individual PTE becomes less. We can also clearly see that the sink phenomenon has been removed significantly. This can be interpreted that there is less mutual coupling and sink phenomenon as constraints are applied. Finally, Figure 34 is the receiver gain with respect to the number of receivers from 1 to 4 when there is only one transmitter in the center of a circle of radius 0.35λ. Since the region of interest is not large enough, although guard spacing of 0.1λ is applied, the more receivers we have, the worse the individual PTE is. The overall PTE has higher value as the number of receivers increases, but the increment is getting smaller, which approaches saturation.

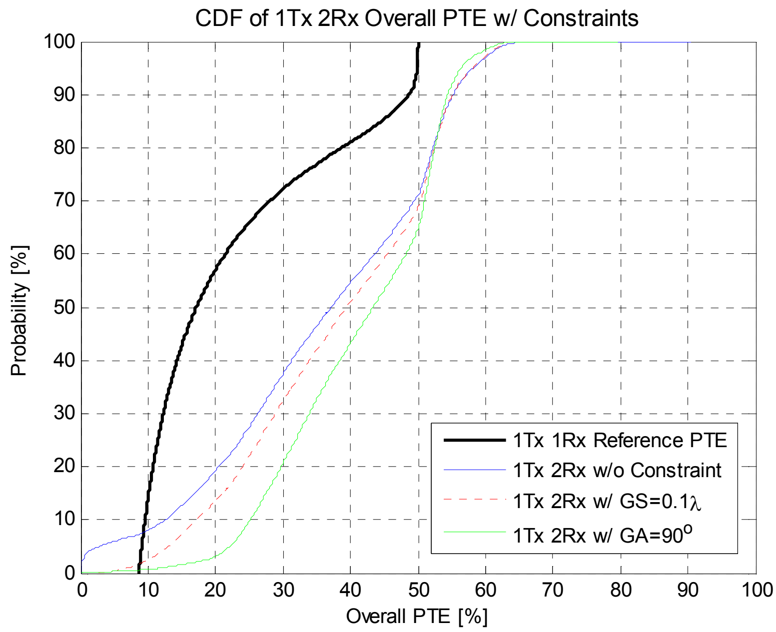

Figure 32. 1Tx 2Rx overall PTE with constraints

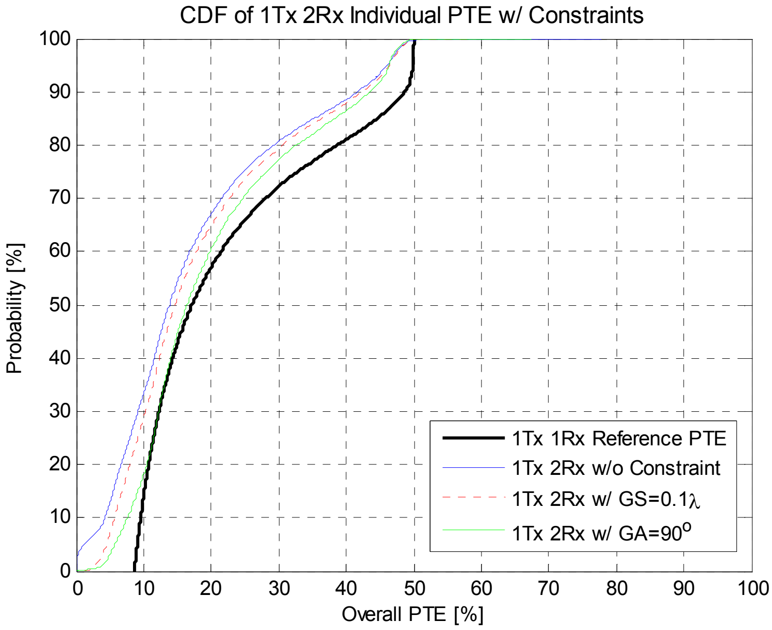

Figure 33. 1Tx 2Rx individual PTE with constraints

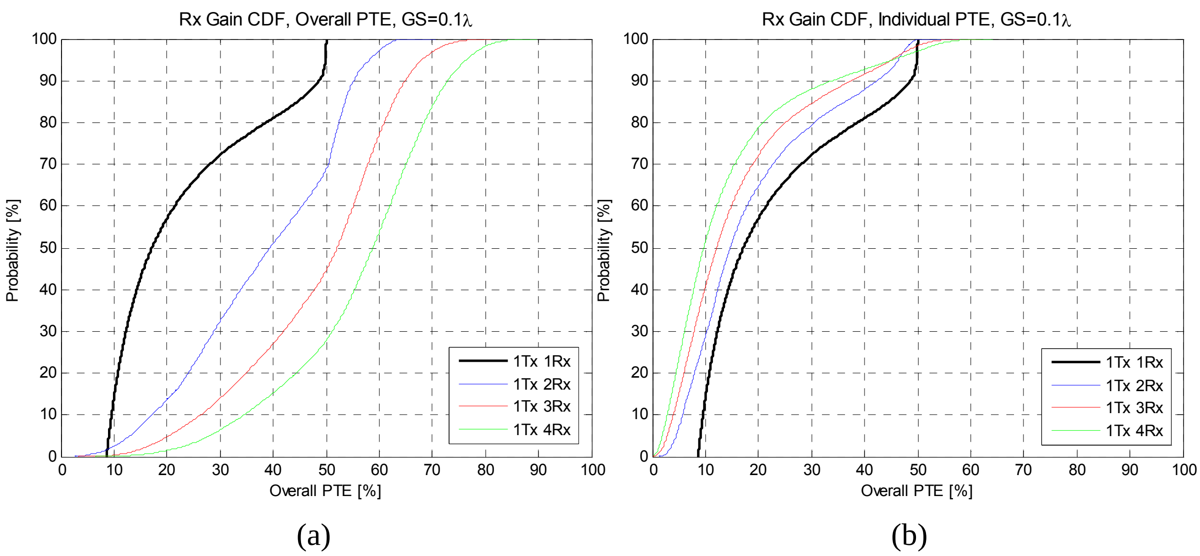

Figure 34. Rx gain. (a) Overall PTE, (b) Individual PTE

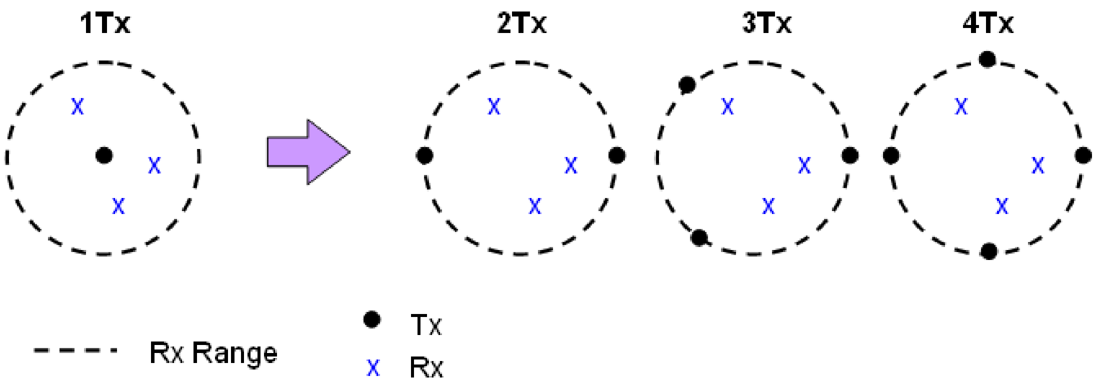

Figure 35. Tx placement scheme 1

4. 5. TRANSMITTER AND RECEIVER DIVERSITY GAIN

Monte-Carlo simulation of multiple transmitters and multiple receivers is presented in this section. For all results, guard spacing of 0.1λ is applied. To boost the overall and individual PTE, adding more transmitters has been considered, but only fixed positions have been applied to transmitters to make the problem simpler. However, to apply fixed positions to transmitters, a specific scheme is needed to place them consistently. The first scheme is depicted in Figure 35. However, scheme 1 does have consistency in changing from 2Tx to 4Tx, but not from 1Tx to 2Tx.

As shown in Table 4 and Figure 37, the PTE of 1Tx is higher than the PTE of 2Tx which does not seem to be right intuitively. To solve this problem, Tx placement scheme 2 has been applied as depicted in Figure 36, and this follows the rule of placing transmitters in the center of divided regions. Therefore, the number of transmitters is the same as the number of divided region.

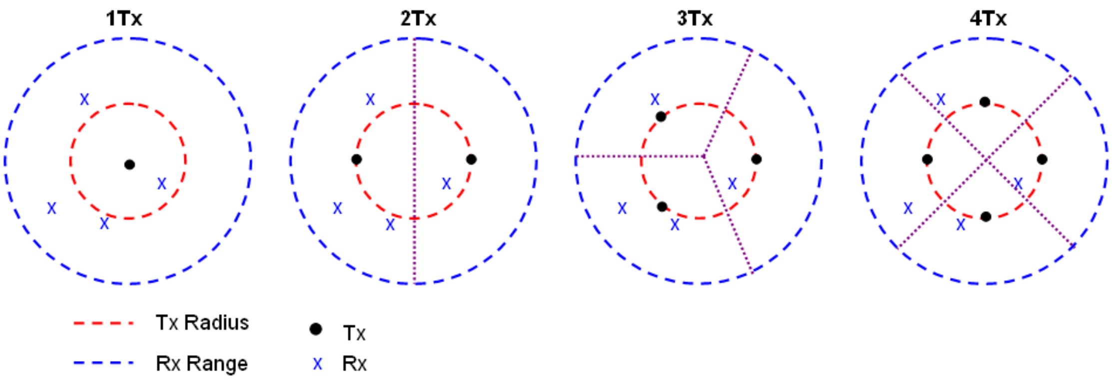

Figure 36. Tx placement scheme 2

	1 Tx	2 Tx	3 Tx	4 Tx
1 Rx	23.0%	21.2%	34.2%	39.1%
	23.0%	21.2%	34.2%	39.1%
2 Rx	38.3%	29.6%	42.7%	46.8%
	19.2%	14.8%	21.4%	23.4%
3 Rx	48.7%	34.1%	47.2%	51.2%
	16.2%	11.4%	15.7%	17.1%
4 Rx	56.4%	38.1%	51.0%	55.0%
	14.1%	9.5%	12.8%	13.8%

Overall PTE (yellow; first row for each Rx)
Individual PTE (blue; second row for each Rx)

Table 4. Average PTE of multiple Tx / Rx. Rx range : 0.35λ, Tx radius : 0.35λ

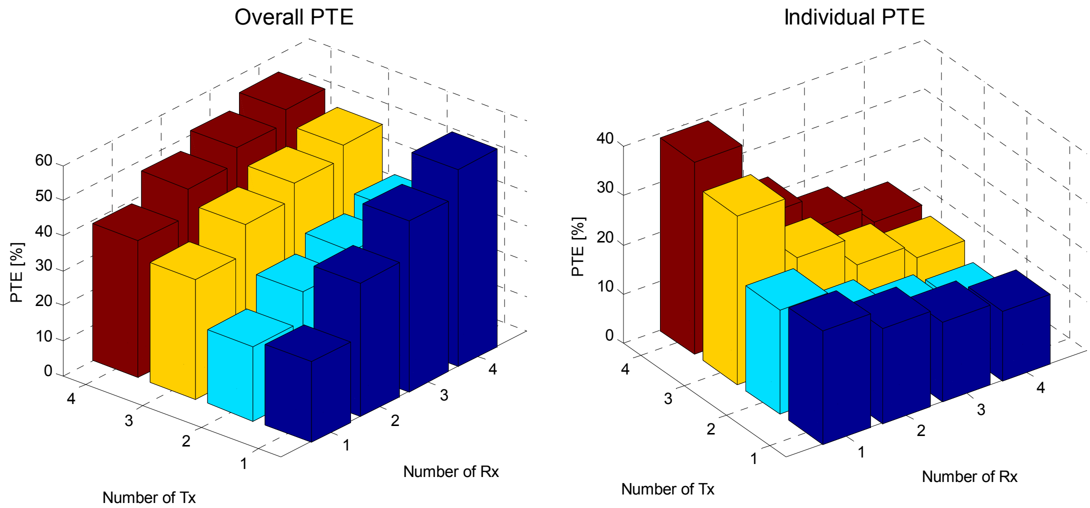

(a) (b)

Figure 37. Diversity gain of Table 4. (a) Overall PTE, (b) Individual PTE

	1 Tx	2 Tx	3 Tx	4 Tx
1 Rx	23.0%	29.3%	32.4%	33.4%
	23.0%	29.3%	32.4%	33.4%
2 Rx	37.8%	43.8%	45.7%	46.3%
	18.9%	21.9%	22.9%	23.2%
3 Rx	48.6%	52.6%	53.8%	53.5%
	16.2%	17.5%	17.9%	17.8%
4 Rx	56.5%	58.7%	59.6%	58.8%
	14.1%	14.7%	14.9%	14.7%

Overall PTE
Individual PTE

Table 5. Average PTE of multiple Tx / Rx. Rx range : 0.35λ, Tx radius : 0.175λ

The case of Tx placement scheme 2 has been simulated with two different configurations of which the results are shown in Table 5 and Table 6 for Rx range 0.35λ / Tx radius 0.175λ and Rx range 0.70λ / Tx radius 0.35λ, respectively. Figure 38 and Figure 40 are corresponding transmitter and receiver diversity gain in 3D bar graphs.

	1 Tx	2 Tx	3 Tx	4 Tx
1 Rx	9.4%	12.0%	17.4%	19.5%
	9.4%	12.0%	17.4%	19.5%
2 Rx	17.6%	21.7%	28.8%	31.8%
	8.8%	10.9%	14.4%	15.9%
3 Rx	24.6%	29.2%	36.9%	40.3%
	8.2%	9.7%	12.3%	13.4%
4 Rx	31.0%	35.6%	43.9%	46.8%
	7.8%	8.9%	11.0%	11.7%

Overall PTE
Individual PTE

Table 6. Average PTE of multiple Tx / Rx. Rx range : 0.70λ, Tx radius : 0.35λ

Now, the problem of scheme 1 seems to be solved with gradually increasing PTE according to the number of transmitters. However, it has been found that the overall PTE does not increase as a factor of N (number of transmitters) linearly, which is intuitively expected when there is nothing prevents the transmitters from delivering power freely to receivers. Furthermore, the transmitter gain is lower than the receiver gain which is already suffering from mutual coupling and a sink phenomenon. Figure 39. (a) and Figure 41. (a) are the transmitter gain with the number of receivers fixed as 1, and Figure 39. (b) and Figure 41. (b) are the receiver gain with the number of transmitters fixed as 1. Red dotted line is the ideal transmitter or receiver gain which is simply N multiplied by the PTE of 1Tx 1Rx case. It is shown that the transmitter gain is more off from the ideal one. However, after a close look at Figure 42 and Figure 43, 2-D plots of multiple transmitters cases, it can be understood that added transmitter only boosts the PTE within limited distance around it. Therefore, the effect of adding transmitters cannot reach to the edge regions which have already poor PTE, and this can be one of possible ways to explain why we cannot expect the ideal transmitter gain. It can be thought of a matter of geometry, and detailed investigation may be a future work of this thesis to find out more efficient placement of transmitters to provide better transmitter gain.

4. 6. SUMMARY

In this chapter, Monte-Carlo simulation was applied to account for more general situations without constraints of receiver positions. To understand the transmitter and the receiver diversity without a simple one-dimensional plot, the PDF and CDF curves were introduced and their interpretations were provided with an example of the case of 1Tx 1Rx. Using the PDF and CDF, we were able to find the diversity gain and the sink phenomenon again. Furthermore, constraints were proposed to reduce PTE degradation due to the sink phenomenon, and their effects were verified from the resulting PDF and CDF curves. Finally, the transmitter and receiver diversity gain showed that there is a saturation in both the transmitter and receiver gain, which means adding more elements does not help boost the PTE beyond a certain number of elements.

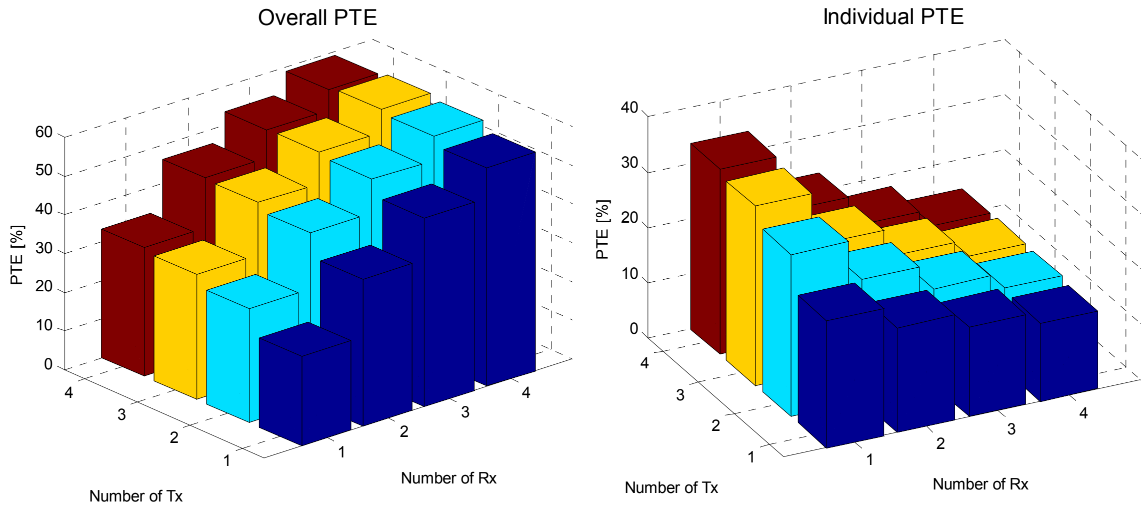

(a) (b)

Figure 38. Diversity gain of Table 5. (a) Overall PTE, (b) Individual PTE

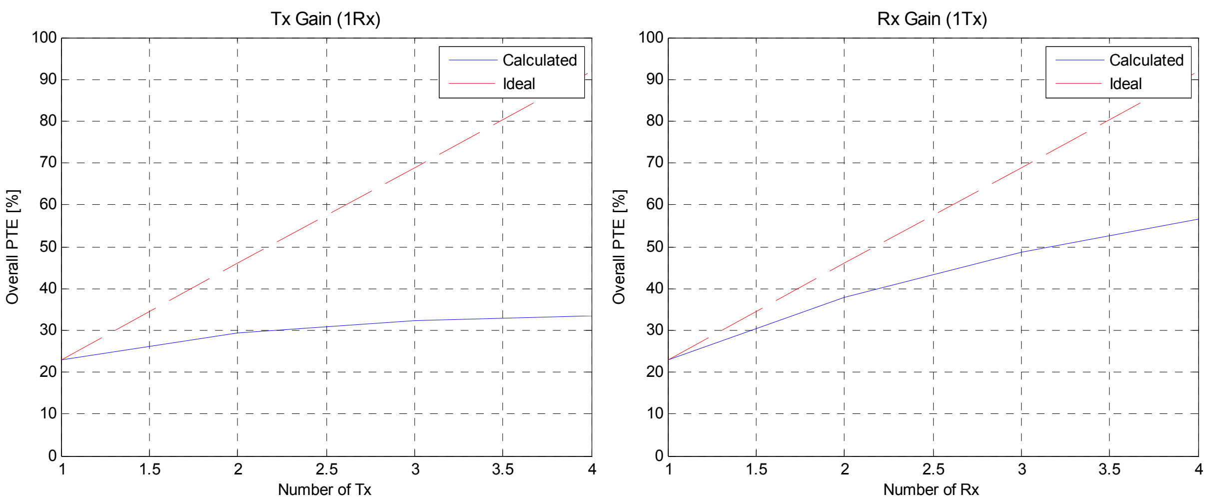

(a) (b)

Figure 39. (a) Tx gain (b) Rx gain of Table 5

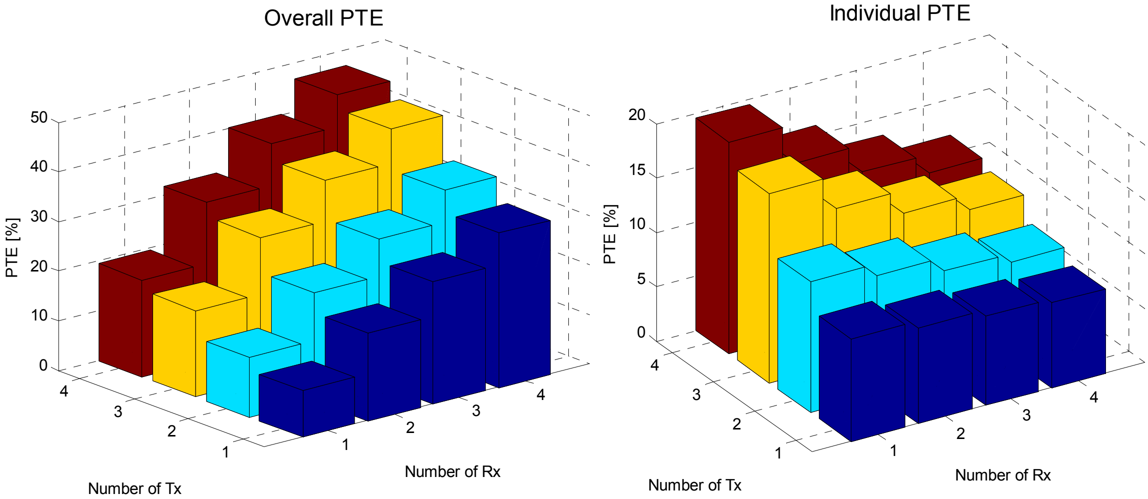

(a) (b)

Figure 40. Diversity gain of Table 6. (a) Overall PTE, (b) Individual PTE

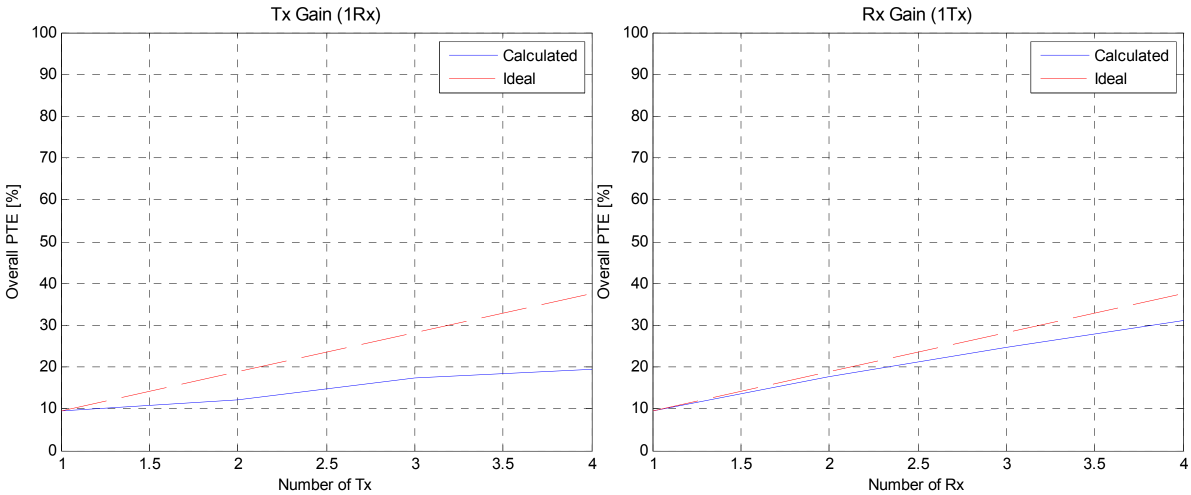

(a) (b)

Figure 41. (a) Tx gain (b) Rx gain of Table 6

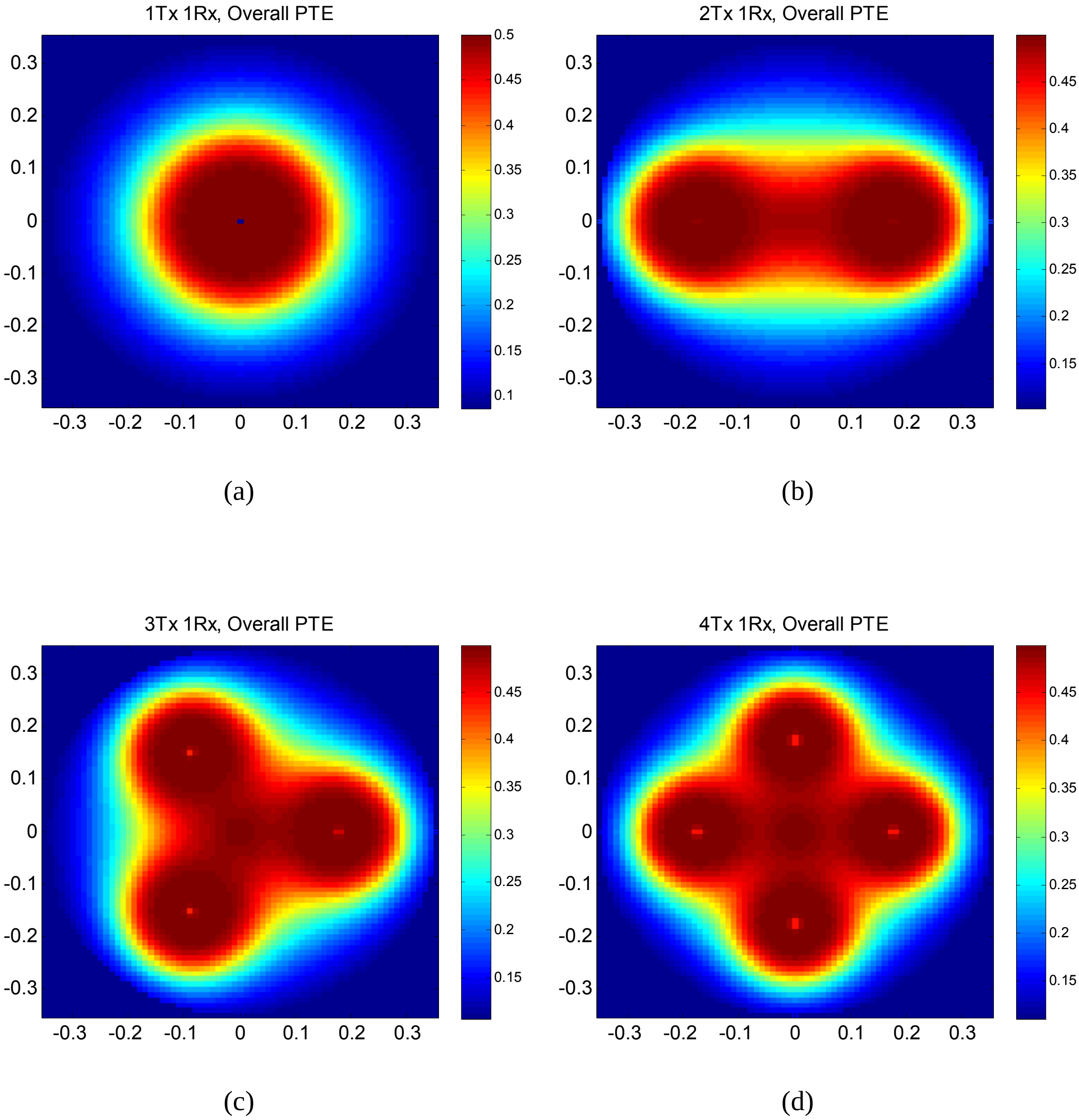

Figure 42. Single Rx PTE 2-D plot for Rx range : 0.35λ, Rx radius : 0.175λ (a) 1Tx 1Rx (b) 2Tx 1Rx (c) 3Tx 1Rx (d) 4Tx 1Rx

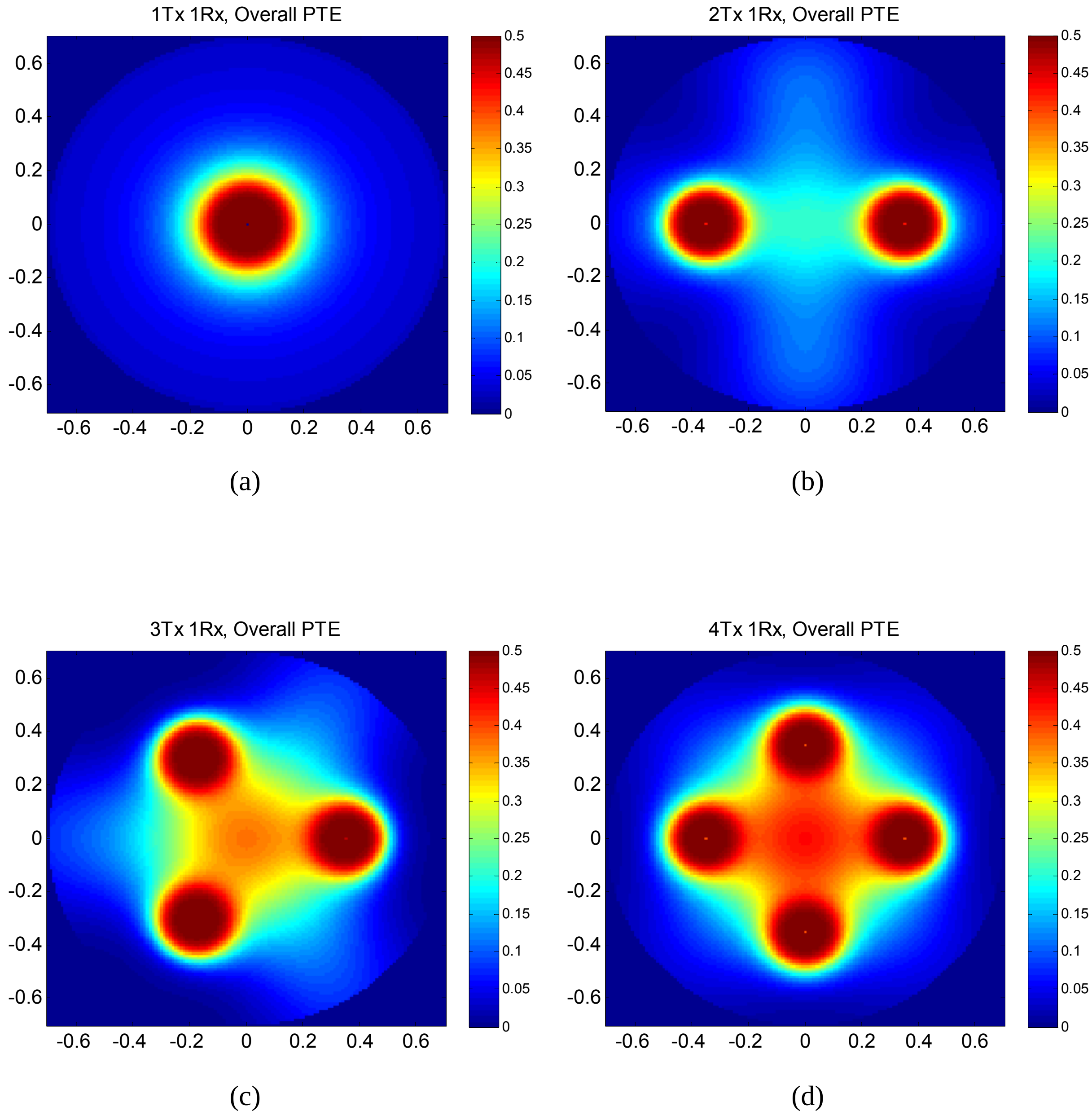

Figure 43. Single Rx PTE 2-D plot for Rx range : 0.70λ, Tx radius : 0.35λ (a) 1Tx 1Rx (b) 2Tx 1Rx (c) 3Tx 1Rx (d) 4Tx 1Rx

Chapter 5 : Conclusions

The transmitter and receiver diversity for wireless power transfer was discussed in this thesis with more detailed investigation on the receiver diversity. In Chapter 2, the methodology for NEC simulation was introduced and correspondence of multiple transmitters and multiple receivers to N-port network was set. A flat PTE region versus distance and resulting transmitter gain was shown using two configurations of multiple transmitters. In Chapter 3, due to increased degrees of freedom, the methodology to investigate the case of multiple receivers was discussed first, followed by PTE versus distance plots. Upon the investigation of the PTE versus the increasing numbers of receivers with fixed distance, mutual coupling between receivers was found and it was termed as a sink phenomenon. To prove the sink phenomenon, the NEC simulation and measurement were done and the measurement results showed a good agreement with simulation results. Moreover, the load mismatch in receivers was assumed for the reason of the sink phenomenon and it was successfully proven by the local optimization with FCH dipoles. In Chapter 4, to fully use the degrees of freedom of positioning receivers, Monte-Carlo simulation was introduced and performed. It was also successfully shown the sink phenomenon and the transmitter and receiver diversity gain. However, it was shown that the transmitter and receiver gain approach saturation beyond a certain number of transmitters or receivers.

Application-wise, this concludes that users are recommended to stay apart by a certain distance to ensure reliable service as long as they are characterized by the same fixed load impedances, since closely located two users cannot receive power normally. Also, the saturation of the transmitter and receiver diversity gain gives us a lesson that adding more transmitters and receivers are not always good. This means, according to the geometry given, we have to find the appropriate number of transmitters and receivers to maximize the user-wise and the system-wise PTE. Future works of this thesis may include investigating rippling behavior of transmitters and receivers, and finding more appropriate geometry to provide better transmitter gain. This will be great help for further research of wireless power transfer in the aspect of applications.

References

[1] J. Gao, "Inductive power transmission for untethered micro-robots," *Proc. 31st Annual Conference of IEEE Industrial Electronics Society (IECON)*, pp. 6-11, 2005.

[2] T. Deyle and M. Reynolds, "Surface based wireless power transmission and bidirectional communication for autonomous robot swarms," *Proc. IEEE Int. Conf. Robot. Autom. (ICRA)*, Pasadena, CA, USA, pp. 1036-1041, May. 2008.

[3] T. Sekitani, M. Takamiya, Y. Noguchi, S. Nakano, Y. Kato, K. Hizu, H. Kawaguchi, T. Sakurai, and T. Someya, "A large-area flexible wireless power transmission sheet using printed plastic MEMS switches and organic field-effect transistors," *Proc. International Electron Devices Meeting (IEDM)*, San Francisco, CA, USA, pp. 1-4, Dec. 2006.

[4] Y. Jang and M. M. Jovanovic, "A contactless electrical energy transmission system for portable-telephone battery chargers," *IEEE Trans. Ind. Electron.*, Vol. 50, No. 3, pp. 520-527, Jun. 2003.

[5] X. Liu and S. Hui, "Optimal design of a hybrid winding structure for planar contactless battery charging platform," *IEEE Trans. Power Electron.*, Vol. 23, No. 1, pp. 455-463, Jan. 2008.

[6] G. B. Joun and B. H. Cho, "An energy transmission system for an artificial heart using leakage inductance compensation of transcutaneous transformer," *IEEE Trans. Power Electron.*, Vol. 13, No. 6, pp. 1013-1022, Nov. 1998.

[7] G. Wang, W. Liu, R. Bashirullah, M. Sivaprakasam, G. A. Kendir, Y. Ji, M. S. Humayun, and J. D. Weiland, "A closed loop transcutaneous power transfer system for implantable devices with enhanced stability," *Proc. IEEE International*

Symposium on Circuits and Systems (ISCAS), Vancouver, Canada, Vol. 4, pp. 17-20, May. 2004.

[8] A. K. Ramrakhyani, S. Mirabbasi, and M. Chiao, “Design and optimization of resonance-based efficient wireless power delivery systems for biomedical implants,” *IEEE Trans. Biomed. Circuits Syst.*, Vol. 5, No. 1, Feb. 2011.

[9] G. A. Covic, J. T. Boys, M. L. G. Kissin, and H. G. Lu, “A three-phase inductive power transfer system for roadway-powered vehicles,” *IEEE Trans. Ind. Electron.*, Vol. 54, No. 6, pp. 3370-3378, Dec. 2007.

[10] T. Imura, H. Okabe, and Y. Hori, “Basic experimental study on helical antennas of wireless power transfer for electric vehicles by using magnetic resonant couplings,” *Proc. IEEE Vehicle Power and Propulsion Conf. (VPPC)*, Dearborn, MI, USA, pp. 936-940, Sep. 2009.

[11] G. Goubau and F. Schwering, “On the guided propagation of electromagnetic wave beams,” *IRE Trans. Antennas Propagag.*, Vol. AP-9, pp. 248-256, May 1961.

[12] W. C. Brown, “Experiments in the transportation of energy by microwave beam,” *IRE Int. Conv. Rec.*, pp. 8-17, Mar. 1964.

[13] W. C. Brown and E. E. Eves, “Beamed microwave power transmission and its application to space,” *IEEE Trans. Microw. Theory Tech.*, Vol. 40, No. 6, pp. 1239-1250, Jun. 1992.

[14] W. C. Brown, “Experiments involving a microwave beam to power and position a helicopter," *IEEE Trans. Aerosp. Electron. Syst.*, Vol. 5, pp. 692-702, Sep. 1969.

[15] W. C. Brown, “Satellite power stations - A new source of energy?,” *IEEE Spectrum*, Vol. 10, No. 3, pp. 38-47, Mar. 1973.

[16] A. Sample and J. R. Smith, "Experimental results with two wireless power transfer systems," *IEEE Radio and Wireless Symposium*, San Diego, CA, USA, pp. 16-18, Jan. 2009.

[17] A. Kurs, A. Karalis, R. Moffatt, J. D. Joannopoulos, P. Fisher, and M. Soljacic, "Wireless power transfer via strongly coupled magnetic resonances," *Science,* Vol. 317, pp. 83-86, Jun. 2007.

[18] A.Karalis, J. D. Joannopoulos, and M. Soljacic, "Efficient wireless non-radiative mid-range energy transfer," *Ann. Phys.*, Vol. 323, No. 1, pp. 34-48, Jan. 2008.

[19] Y. Kim and H. Ling, "Investigation of coupled mode behavior of electrically small meander antenna," *IET Electron. Lett.*, Vol. 43, pp. 1250-1252, Nov. 2007.

[20] Y. Kim and H. Ling, "On the coupled mode behavior of electrically small antennas," *Proc. URSI Nat. Radio Sci. Meeting*, San Diego, CA, Jul. 2008.

[21] J. Lee and S. Nam, "Fundamental aspects of near-field coupling small antennas for wireless power transfer," *IEEE Trans. Antennas Propag.*, Vol. 58, pp. 3442-3449, Aug. 2010.

[22] I. -J. Yoon and H. Ling, "Realizing efficient wireless power transfer using small folded cylindrical helix dipoles," *IEEE Antennas Wirel. Propag. Lett.*, Vol. 9, pp. 846-849, 2010.

[23] S. R. Best, "A comparison of the cylindrical folded helix Q to the Gustafsson limit," *Proc. EuCAP*, Berlin, Germany, pp.2554-2557, Mar. 2009.

[24] S. R. Best, "The quality factor of the folded cylindrical helix," *Radioengineering*, Vol. 18, No. 4, pp.343-347, Dec. 2009.

[25] B. L. Cannon, J. F. Hoburg, D. D. Stancil, and S. C. Goldstein, "Magnetic resonant coupling as a potential means for wireless power transfer to multiple small receivers," *IEEE Trans. Power Electron.*, Vol. 24, No. 7, pp. 1819-1825, Jul. 2009.

[26] A. Kurs, R. Moffatt, and M. Soljacic, "Simultaneous mid-range power transfer to multiple devices," *Appl. Phys.* Lett. Vol. 96, 044102, 2010.

[27] I. -J. Yoon, B. W. Jun, and H. Ling, "Near-field wireless power transfer under multiple transmitter and multiple receiver scenarios," Accepted for presentation in *URSI Nat. Radio Sci. Meeting*, Spokane, WA, Jul. 2011.

[28] J. J. Casanova, Z. N. Low, and J. Lin, "A loosely coupled planar wireless power system for multiple receivers," *IEEE Trans. Ind. Electron.*, Vol. 56, No. 8, pp. 3060-3068, 2009.

[29] D. Rubin, "The Linville method of high frequency transistor amplifier design", *Naval Weapons Center, Research Department*, *NWCCL TP 845*, Corona Laboratories, Corona, California, March 1969.

[30] C. A. Balanis, *Antenna Theory: Analysis and Design*, John Wiley & Sons, 3rd Ed., 2005.

[31] C. A. Levis, J. T. Johnson, and F. L. Teixeira, *Radiowave Propagation Physics and Applications*, John Wiley & Sons, 2010.

[32] D. Pozar, *Microwave Engineering*, John Wiley & Sons, 3rd Ed., 2005.